QUANTUM TRANSPORT IN NANOSTRUCTURED MATERIALS

A Thesis Submitted to
the Graduate School of Engineering and Sciences of
İzmir Institute of Technology
in Partial Fulfillment of the Requirements for the Degree of

MASTER OF SCIENCE

in Materials Science and Engineering

by
Gizem KURT

July 2017
İZMİR

We approve the thesis of **Gizem KURT**

Examining Committee Members:

Assoc. Prof. Dr. Hâldun SEVİNÇLİ
Department of Materials Science and Engineering, İzmir Institute of Technology

---

Assoc. Prof. Dr. Özgür ÇAKIR
Department of Physics, İzmir Institute of Technology

Prof. Dr. R. Tuğrul SENGER
Department of Physics, İzmir Institute of Technology

Prof. Dr. Mustafa M. DEMİR
Department of Materials Science and Engineering, İzmir Institute of Technology

---

Assoc. Prof. Dr. Ethem AKTÜRK
Department of Physics, Adnan Menderes University

25 July 2017

Assoc. Prof. Dr. Hâldun SEVİNÇLİ
Supervisor, Materials Science and Engineering
İzmir Institute of Technology

Assoc. Prof. Dr. Özgür ÇAKIR
Co-Supervisor, Department of Physics
İzmir Institute of Technology

Prof. Dr. Mustafa M. DEMİR
Head of the Department of
Materials Science and Engineering

Prof. Dr. Aysun SOFUOĞLU
Dean of the Graduate School of
Engineering and Sciences

ACKNOWLEDGMENTS

I would like to thank my supervisor Assoc. Prof. Hâldun SEVİNÇLİ for his great contribution. I would like to thank other members of my defence committee, Prof. Dr. R. Tuğrul SENGER, Prof. Dr. Mustafa M. DEMİR, Assoc. Prof. Dr. Özgür ÇAKIR, and Assoc. Prof. Dr. Ethem AKTÜRK for worthwhile suggestions and comments.

I sincerely feel thankful to İdil Merve KARAOĞLU for her priceless support while I was writing my thesis. I relied heavily on her knowledge of the English language. I am also grateful to İlknur BEYAZ for her contributions to the language.

I would like to thank Tuğce SEMERCİ for her graphical contribution. I feel thankful to Gündeniz AKKOÇ, Ayşegül GÜMÜŞ, Merve GENÇOĞLU, Öykü TANIŞMAN, Birnur KAYA, and Mustafa Neşet ÇINAR. I also feel thankful to Damlasu ÇEŞMECİ due to being my psychic gibbon during nervous time of thesis. Finally, I would like to express my gratitude to my family.

ABSTRACT

QUANTUM TRANSPORT IN NANOSTRUCTURED MATERIALS

Due to the advances in the measurement and fabrication techniques at the nano-scale it is now possible to measure thermal transport across single molecule junctions[1], which makes it possible to consider nano-scale thermal devices. One of the building blocks for such thermal devices should be thermal switches. The aim of this study is to design a thermal switch, which is based on a single molecule junction and photoisomerism. We propose reversible photoisomerism as a key ingredient to build reversible thermal switches based on single molecule junctions. In this thesis, the thermal conductances of molecular junctions built by azobenzene and its derivatives are computed using density functional theory based tight binding method combined with atomistic Green's functions. These molecules show photoisomeric behaviour by switching their three-dimensional structure when exposed to radiation. We investigate the effects of different linker groups as well as the details of the reservoirs. Carbon nanotubes are used as reservoirs, while generic reservoirs are also investigated to illuminate the effects of the reservoir details. We show that thermal conductance can be altered by switching the molecule from *trans* to *cis* configuration. The effect is robust under the change of the linkers that bind the molecules to the reservoirs and under the change of the particular molecular species.

ÖZET

NANO SEVİYE MALZEMELERDE KUANTUM TAŞINIMI

Nano düzeydeki ölçüm ve üretim tekniklerindeki gelişmeler sayesinde, tek moleküllü eklemlerde ısıl taşınım ölçümü günümüzde mümkündür[1], bu durum nano ölçekte termal cihazlar yapımını mümkün kılar. Termal cihazların yapıtaşlarından biri ise ısısal anahtardır. Bu çalışmanın amacı ise fotoizomerleşmeye ve tek moleküllü eklemlere dayanan bir ısıl anahtar yapmaktır. Tersinir fotoizomerleşme tek moleküllü eklemlere dayanan tersinir ısıl anahtar yapımının asli unsurudur. Bu tezde, azobenzen ve türevlerinden kurulan moleküler eklemlerin ısıl iletkenlikleri atomistik Green fonksiyonları ile kombine edilmiş yoğunluk fonksiyoneli teorisine dayanan sıkıbağlanma methodu kullanılarak hesaplanmıştır. Bu moleküller fotoizomerleşme özelliğini ışık altında uzaydaki üç boyutlu yapısını değiştirerek göstermektedirler. Rezervuar detaylarının yanı sıra farklı bağlayıcı grupların etkileri araştırılmıştir. Rezervuar olarak karbon nanotüpler kullanılmıştır, ve bununla beraber rezervuar detaylarının etkilerini incelemek için jenerik rezervuarlar da incelenmiştir. Isıl iletkenliğin molekülün yapısının *trans* konfigurasyondan *sis* konfigurasyonuna geçişinden dolayı değişebileceğini gösterilmiştir. Bu değişim molekülü rezervuara bağlayan bağlayıcı grupların degiştirilmesi durumunda da ve molekülün değişmesi durumunda da gözlenmektedir.

To my daughter..

TABLE OF CONTENTS

LIST OF FIGURES

LIST OF TABLES

LIST OF SYMBOLS

SYMBOL	EXPLANATION
$\hat{H}$	Hamiltonian
ω	Angular Frequency
θ_D	Debye temperature
ν	Frequency ($\omega = 2\pi\nu$)
v_s	sound velocity
v_g	group velocity
F	Force
C	Force Constants
$\boldsymbol{k}$	wave vector
k_B	Boltzman Constant
h	Planck Constant
$\hbar$	reduced Planck's Constant ($\hbar = h/2\pi$)
T	Temperature
M	Atomic mass
ψ	Wavefunction
ϕ	Nuclear wavefunction
χ	Electronic Wavefunction
Θ	Kohn Sham orbitals
E	Energy

SYMBOL	EXPLANATION
K	Kinetic energy
V	Potantial Energy
U	Total interatomic potential
ρ	Density
$\hat{D}$	Dynamic Matrix
τ	Interaction matrices
g	free Green's function
G	contacted Green's function
Z	Atomic number
$\boldsymbol{r}, \boldsymbol{R}$	Distance between electrons, nuclei
u	vibrational degrees of freedom on displacements
Γ	Broadening
Σ	Self-energy
Ξ	Transmission
f	Bose-Einstein distirbution function
κ	Conductance
SE	Switching effect

LIST OF ABBREVIATIONS

ABBREVATION	EXPLANATION
DFT	Density functional Theory
DFTB	Density functional tight binding
CNT	Carbon nanotube
A-CNT	Armchair carbon nanotube
Z-CNT	Zigzag carbon nanotube
LCB	Left contact bulk region
RCB	Right contact bulk region
AGF	Atomistic Green's Function

CHAPTER 1

INTRODUCTION

1.1. Quantum Thermal Transport

In our time, miscellaneous technological devices are based on miniaturization of their constructional components, such as transistors, diodes, memory chips, switches. Components are getting increasingly smaller. The most important advantage of miniaturization is that the number of components packed on a single chip increases incrementally. Today's technology generates chips in which billions of transistors are embedded. This advancement enables us to produce fast, multi-functional, and small devices. Minimizing the size of systems to nanometer leads to quantum mechanics that depart from classical mechanics primarily with regard to length scales.

Until 1920's, many physicists had thought that most of the important laws of nature had already been explored. However, the strange behaviour of the blackbody spectrum, namely the ultraviolet catastrophe, and experimental observation of the photoelectric effect, forced physicists to think differently. These phenomenons are incomprehensible to classical physics, although it describes macroscopic worlds successfully. According to classical physics, energy of light depends on its intensity, and all energies are allowed. On the contrary, photoelectron emission does not occur until the frequency of the light is high enough, which means that the energy of light depends on its frequency. Additionally, within the classical theory, the mean energy of any oscillator is $k_B T$. Blackbody radiation showed that actual average energy is $\epsilon = h\nu/(\exp(h\nu/k_B T) - 1)$. These results led to the discovery of quanta, which refers to discrete packets of energy. According to quantum theory, each photon, which is a small packet of light, with the frequency 'ν ' has the energy of Planck's constant multiplied by its frequency, $h\nu$. The energy emitted from the oscillators of the blackbody walls can have discrete energies

$$\epsilon_n = nh\nu \qquad n = 0, 1, 2, ... \tag{1.1}$$

and the mean value of energy is no longer average of oscillators energies which display

continuous distribution, instead average of

$$\epsilon = \frac{h\nu}{e^{\frac{h\nu}{k_B T}} - 1} \tag{1.2}$$

Quantum theory has successfully clarified the strange behaviour of blackbody spectrum and the photoelectric effect with this new quantization perspective. The most direct evidence to observe discrete energy is energy spectrum of atoms. [2, 3]

Classical theory also fails to describe the nature of solids within the low temperature limit. It considers the solids as an aggregation of non-interacting harmonic oscillators. By using the equipartition theorem, for each degree of freedom where energy can be stored the energy of one half $k_B T$ is obtained. Within solids, each atom has six degrees of freedom as well as the energy of $3k_B T$. Energy of a solid is the sum of energies of each atom of the solid, $3Nk_B T$. In addition, occupations are governed by the Maxwell-Boltzmann distribution function of classical statistical mechanics. This result established by Mr. Boltzmann in 1896 was an extremely important result for a number of reasons. Firstly, the result revealed the law of Dulong-Petit that had been known for almost a hundred of years without knowledge of its reason. The law of Dulong-Petit states that internal energy of most solids is constant $3Nk_B T$, and it is based on experimental observations. Moreover, the result was extremely important since it revealed the validity of statistical mechanics. However, there was a problem, the law of Dulong-Petit is not always valid. There were significant deviations from the law at low temperatures. The source of problem was identified by Einstein. Einstein treated the oscillators using quantum mechanics rather than classical mechanics. He incorporated the quantization perspective to the Boltzmann solids [4]. Due to the quantum mechanics, the energy levels of a harmonic oscillator are quantized, and the energy states of an atom in the harmonic well is $E_n = h\nu(n + 1/2)$, where the quantum number, n, is a non-negative integer. This is the result of one-dimensional oscillators. Hence the avarage energy per oscillator is the same as in equation 1.2. The energy of a solid became

$$E = \frac{3Nh\nu}{e^{\frac{h\nu}{k_B T}} - 1} \tag{1.3}$$

Although, the Einstein model clarifies the deviations from the law of Dulong-Petit at low temperatures, it can not make an exact quantitative agreement with the experimental val-

ues. The inadequacy of the Einstein model brought out the subject of today, which is the Debye model of solids. The Debye's intuition was that solids can not be thought as a bunch of non-interacting harmonic oscillators because when an atom moves, it does get a push-back to its original position by its neighbour. But, in the process it pushes its neighbour, and the neighbour pushes its neighbour, so forth [5]. So, in fact, the vibration in a solid is actually a wave, and each wave mode in a solid should be treated as an oscillator. Based on Einstein's work, the energy of a given oscillator would be $E_n = h\nu(n + 1/2)$. According to the Debye model, a solid can be considered as a box. The total energy of a solid is the sum over all the wave modes in the box [6]. Such intuition differs from Einstein's in that whenever there is a bunch of modes in a box, some of those modes are going to be low energy (frequency) modes. The poor fit of the Einstein model originates from his assumption, which claims that atoms oscillate independently at fixed frequency. Due to the Debye model, there is a finite number of modes. The cut-off frequency is equal to the Debye frequency, which is determined by the interatomic forces between atoms. The Debye frequency of a solid describes the possible maximum frequency of phonons which propagate through that solid. There is no wave mode above the Debye frequency. The Debye temperature is $\hbar\omega_D/k_B$ where ω_D is the Debye frequency. The materials in which atoms are bound tightly to each other have higher Debye temperatures. It can be related to the hardness of a material as well as the bond strength. For instance, carbon materials have high Debye Temperatures. Below the Debye temperature, quantum effects are significant since thermal energy, k_BT, is lower than the gap between the discrete energy levels. It is necessary to use quantum statistics within this limit. Bose-Einstein distribution function, $(1/(e^{(\hbar\omega/k_BT)} - 1))$, defines the filling of states of bosons which are particles with integer spin. Within the low temperature limit, Bose-Einstein distribution function vanishes very quickly to zero. At high temperatures where $\hbar\omega/k_BT$ is a small number Bose Factor can be replaced by

$$\frac{1}{(e^{(\hbar\omega/k_BT)} - 1)} = \frac{1}{(1 + \frac{\hbar\omega}{k_BT}) - 1} = \frac{1}{\frac{\hbar\omega}{k_BT}} \tag{1.4}$$

Since the Taylor series expansion of exponential functions is

$$e^x = 1 + x + \frac{1}{2!}x^2 + ... \tag{1.5}$$

All terms of order higher than the first-order can be ignored. By this substitution, the difference between quantum behaviour and classical behaviour vanishes. Occupations of bosons increase linearly with temperature. [7].

1.2. Phonons

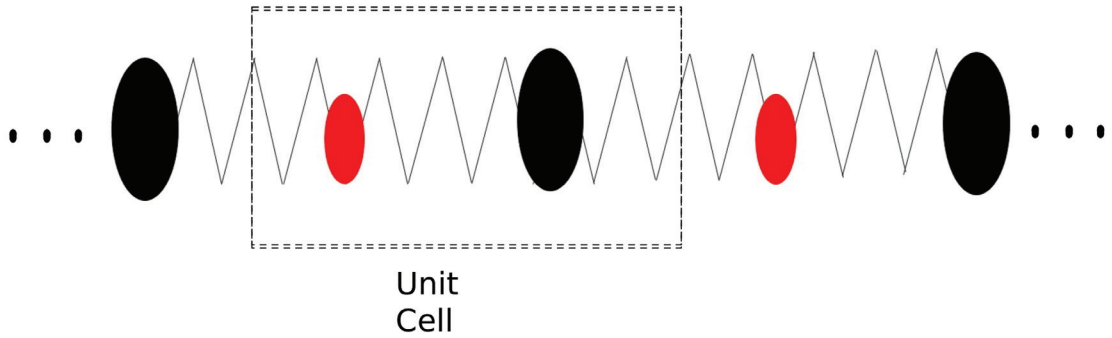

Figure 1.1. Illustration of a one-dimensional linear chain and its unit cell. This unit cell consists of two different kinds of atoms.

In crystal structures, atoms are located in a repetitive lattice. The bonds, which hold atoms together, behave like springs as mentioned in the previous section. As a result, atoms oscillate at certain frequencies. Phonons are quantized lattice waves, and the lattice waves are collective vibrational motions of atoms. Phonons are the carriers of heat and sound. Unlike light waves, which have two polarizations, phonons have three polarizations: one longitudinal, two transverse. In longitudinal waves, atoms move back and forth along the direction of propagation of the phonon. In transverse waves, atoms move up and down in regard to the direction of propagation.

The simplest example to basically comprehend phonons is one-dimensional linear chain. In a crystalline solid, due to the repetitive layout of atoms, the motions of the atoms can be characterized by solely considering its smallest repeating unit, namely unit cell. Figure 1.1 illustrates a unit cell which consists two different atoms. Solids display two different kinds of phonons, i.e. acoustic phonons and optical phonons. Acoustic branches of phonons are the consequence of in-phase movements of atoms, while optical branches are the consequence of out-of-phase movements. All solids display acoustic branches of phonons, while optic branches of phonons occur only if there is more than

one atom in its unit cell. Acoustic waves have similar characteristics with sound waves. An electric field with proper frequency can actuate an optical phonon. This is the reason why it is called optical phonon. Phonons are represented by the relationship between the wavevector and the frequency which is called the dispersion relation, $w(\boldsymbol{k})$, where $\boldsymbol{k}$ is the wavevector of a phonon. The number of phonon branches depends on the number of atoms inside its unit cell, therefore if there are n atoms inside unit cell, corresponding bulk structure displays $3n$ phonon dispersion branches. In two and three-dimensional solids, three of them are acoustic and rest are optical, while in one-dimensional solids, four are acoustic and the rest are optical. The common three acoustic branches emerge from in-phase movements of atoms along X-axis, Y-axis, and Z-axis of the coordinate system. An additional acoustic branch, which is only observed in one-dimensional solids, is caused by the coherent torsional motion of atoms. [7–9]

1.3. Phononics

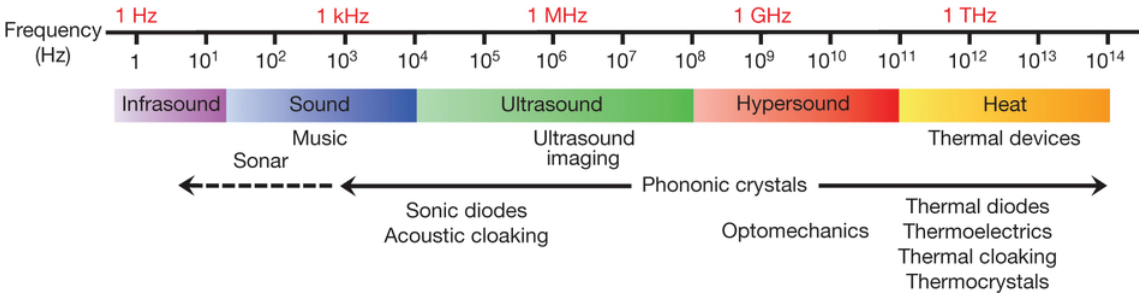

Figure 1.2. Illustration of the phononic spectrum The figure is adapted from the reference [10].

Phononics is the science of controlling and managing phonons. Admittedly, control of the energy carried by phonons is indeed more difficult than control of the energy carried by photons and electrons. This is because phonons are quasi-particles in the form of energy, and they possess neither a charge nor mass. However, due to the advancements in the measurement and fabrication techniques at the nano-scale, it is now possible to measure thermal transport across a single atom junction [1], which makes it possible to consider nano-scale thermal devices. Understanding the nature of phonons and improving our ability to control phonons provide opportunities to construct thermally insulated buildings, reduce environmental noise, transform waste heat energy into electricity, and

develop earthquake protection (see Figure 1.2) [11], but phonons play a secondary role in these applications. In addition to these, most of opportunities achieved by controlling electrons and photons can also be achieved by controlling phonons [12, 13]. Such possibilities would have potential applications in nano-scale thermal molecular devices such as thermal logics, thermal rectifiers, logic gates, thermal memories, and thermal transistors.

In molecular phononics, like molecular electronics, molecules instead of bulk materials are used as components of the system, and to yield active and passive components such as switches, diodes etc. Molecular phononics involves the use of a single molecule or small packets of molecules as units for computing.

1.4. Statement of the Problem: Phononic switch

The demand of thermal management in science and industry is rapidly growing [14, 15], not only due to the requirement to invest in altarnetive energy sources [13], but also in order to get rid of dissipative heat from components [16]. Researchers widely investigate the opportunities to take control of thermal flow. Managing thermal conductivity by the virtue of the material's design is a remarkable issue to build thermal devices. Thermal switch is one of the building blocks of thermal devices. A thermal switch would greatly improve our ability to control heat flow since it alters the thermal conductances between ”on” and ”off” state [10, 17]. The construction of a thermal switch is a widely studied phenomenon [18–21].

Photoisomeric molecules attract considerable attention since these molecules give opportunities to build systems whose properties can be controlled by light. There is a great amount of researches about possible applications of photoisomeric molecules. In this study, the possibility of management of thermal conductivity by photoisomeric behaviour of azobenzene and its derivatives is going to be investigated. The thesis is organized as follows: Chapter 2 explains the methods, and defines theoretical background information the methods rely on. Chapter 3 defines the system set-up from molecules to construction of the switch. Numerical results are analysed in chapter 4. Finally, chapter 5 presents the conclusion.

CHAPTER 2

METHODS

2.1. Density Functional Theory

In physics, the answer of most problems associates with the ground state structure. The ground state of any quantum system is the lowest eigenstate of its Hamiltonian.

$$\hat{H}\psi(\boldsymbol{r}_1, \boldsymbol{r}_2, ..., \boldsymbol{r}_N, \boldsymbol{R}_1, \boldsymbol{R}_2, ..., \boldsymbol{R}_M) = E\psi(\boldsymbol{r}_1, \boldsymbol{r}_2, ..., \boldsymbol{r}_N, \boldsymbol{R}_1, \boldsymbol{R}_2, ..., \boldsymbol{R}_M) \quad (2.1)$$

where E is the lowest eigenvalue. Because most of the Hamiltonian can not be solved exactly the idea of an approximate solution has emerged. The many body Hamiltonian is

$$\hat{H} = -\frac{1}{2}\sum_{i=1}^{N} \bigtriangledown_i^2 - \frac{1}{2}\sum_{A=1}^{M} \frac{1}{M_A} \bigtriangledown_A^2 - \sum_{i=1}^{N}\sum_{A=1}^{M} \frac{Z_A}{\boldsymbol{r}_{iA}} + \sum_{i=1}^{N}\sum_{j\rangle i}^{N} \frac{1}{\boldsymbol{r}_{ij}} + \sum_{A=1}^{M}\sum_{B\rangle A}^{M} \frac{Z_A Z_B}{\boldsymbol{R}_{AB}} \quad (2.2)$$

The terms, from left to right in the above equation, stand for the kinetic energy of electrons, the kinetic energy of nuclei, the attractive forces between electrons and nuclei, the repulsive forces between electrons, and the repulsive forces between nuclei. Equation 2.2 is written in atomic units to avoid inconvenient combinations of the fundamental constants. The abbreviated illustration for the Hamiltonian is

$$\hat{H} = K_{II} + K_{ee} + V_{Ie} + V_{ee} + V_{II} \quad (2.3)$$

and is written in the same order as described in the explanation above.

The first approximation to simplify the Hamiltonian is the adiabatic approximation (the Born-Oppenheimer approximation). The approximation assumes that the nuclei are fixed in positions due to the fact that nuclei are much slower than electrons. As a result the kinetic energy term of nuclei can be neglected, and the nuclear potential term, V_{II}, is constant. A constant potential just shifts the eigenvalues of the Hamiltonian. In addition the electrons feel a static electric potential, V_{Ie}, resulting from the nuclei in that

fixed configuration [22]. The Born-Oppenheimer approximation allows us to separate the system wavefunction into the nuclear wavefunction, ϕ, and the electronic wavefunction, χ.

$$\psi(\boldsymbol{R}, \boldsymbol{r}) = \phi(\boldsymbol{R})\chi(\boldsymbol{r}, \boldsymbol{R}) \tag{2.4}$$

The electronic wavefunction now depends parametrically on the nuclear coordinates rather than the nuclear wavefunction. In other words, dependency of the electronic motion on the nuclear motion, namely decoupling, disappears.

The non-interacting electron approaches, the Hartree and the Hartree-Fock approximation, follow the Born-Oppenheimer approximation [23]. The Hartree approximation assumes that the overall electronic wavefunction is made of individual wavefunctions, so if system has N electrons, electronic wavefunction can be written as a product of individual electronic wavefunctions.

$$\chi(\boldsymbol{r}_1, \boldsymbol{r}_2, ..., \boldsymbol{r}_n) = \chi_1(\boldsymbol{r}_1)\chi_2(\boldsymbol{r}_2).....\chi_N(\boldsymbol{r}_N) \tag{2.5}$$

is called the Hartree product. Therefore, the Hamiltonian can be written like the one-electron Schrödinger equation

$$\hat{H}_H\chi_i(\boldsymbol{r}, \boldsymbol{R}) = \epsilon_i\chi_i(\boldsymbol{r}, \boldsymbol{R}) \tag{2.6}$$

$$\hat{H}_H = -\frac{1}{2}\bigtriangledown_i^2 + V(\boldsymbol{r}, \boldsymbol{R}) \tag{2.7}$$

with the potential, $V(\boldsymbol{r}, \boldsymbol{R}) = V_{Ie}(\boldsymbol{r}, \boldsymbol{R}) + V_{ee}(\boldsymbol{r})$, and each electron is under a mean-field Coloumb potential arising from the remaining $N - 1$ electrons.

$$V_{Hartree}(\boldsymbol{r}) = \frac{1}{2}\int d\boldsymbol{r}'\rho(\boldsymbol{r}')\frac{1}{|\boldsymbol{r} - \boldsymbol{r}'|} \tag{2.8}$$

where $\rho(\boldsymbol{r}') = \sum_i |\chi(\boldsymbol{r})|^2$. The Hartree-Fock approximation can be considered as the Hartree approximation along the exchange effect. The Hartree product fails to reflect the Pauli exclusion principle, which is one of the important elements of essential physics. According to the exclusion principle, wavefunctions of fermions are required to be anti-symmetric. When two electrons are exchanged, the total wavefunction label changes.

$$\psi(\boldsymbol{r}_1, \boldsymbol{r}_2, ..., \boldsymbol{r}_N) = -\psi(\boldsymbol{r}_2, \boldsymbol{r}_1, ..., \boldsymbol{r}_N) \tag{2.9}$$

Formation of the Slater determinant from individual electronic wavefunctions fulfils the requirement of being antisymmetric under the condition of exchange.

$$\chi(\boldsymbol{r}_1, \boldsymbol{r}_2, ..., \boldsymbol{r}_n) = \frac{1}{\sqrt{N!}} \left|\chi_1(\boldsymbol{r}_1)\chi_2(\boldsymbol{r}_2).....\chi_N(\boldsymbol{r}_N)\right| \tag{2.10}$$

It is obvious that the Hamiltonian is also modified due to requirement to fulfil this antisymmetry condition. The exchange term is added to the Hamiltonian. It looks like the Coulomb potential, but describes the exchanged electrons.

$$H_{HF} = -\frac{1}{2} \bigtriangledown_i^2 + V(\boldsymbol{r}, \boldsymbol{R}) - \frac{1}{2} \sum_{i,j} \int d\boldsymbol{r}' \frac{\chi_j^*(\boldsymbol{r}')\chi_i(\boldsymbol{r}')}{|\boldsymbol{r} - \boldsymbol{r}'|} \tag{2.11}$$

The last term is the difference between the so called Hartree Hamiltonian, equation 2.7, and the so called Hartree-Fock Hamiltonian, equation 2.11. As a result, the requirement of the antisymmetry condition is satisfied with this term.

Computational time of the Hartree frame increases according to the augmentation of the number of particles of the system, and in addition the computation is getting more complicated. There are two types of approaches to solve approximately the many body Hamiltonian: Wavefunction based, and density based. The Hartree method and the Hartree-Fock method are two wavefunction based approaches. Density functional theory (DFT) is a density based method. Using density instead of wavefunctions accelerates algorithms.

DFT is based on two theorems proved by Hohenberg and Kohn [24] and the set of equations derived by Kohn and Sham [25]. DFT's name comes from its starting point which is the first theorem proved by Hohenberg and Kohn. The first theorem of Hohenberg-Kohn is that the ground state energy is a particular functional of electronic density. In other words, in the absence of degeneracy, every unique ground state density has its own specific potential, or more explicitly, there is one-to-one correspondence between the ground state density and potential.

$$\rho(\boldsymbol{r}) \Leftrightarrow V(\boldsymbol{r}) \tag{2.12}$$

To understand the theorem, the meaning of functional should be known firstly. A function describes one-to-one relationship between its input and output. A functional is a function

of a function,

$$f(x) = x \rightarrow y \qquad function$$
$$F[(x)] = f(x) \rightarrow y \qquad functional$$

and the density functional means that the ground state energy of a system is the functional of its density, $E[(\rho(\boldsymbol{r}))]$.

The proof of the theorem is simple and based on method of reductio ad absurdum. Assume two different potentials, $V_{xx}(\boldsymbol{r})$ and $V_{yy}(\boldsymbol{r})$, and these two potentials differ from each other more than a constant, and lead to same density, $\rho(\boldsymbol{r})$, in the case of non-degeneracy. The corresponding Hamiltonians, $\hat{H}_{xx}(\boldsymbol{r})$ and $\hat{H}_{yy}(\boldsymbol{r})$, also give rise to the same density, $\rho(\boldsymbol{r})$.

$$E_{xx} \neq \langle \psi_{yy} | \hat{H}_{xx} | \psi_{yy} \rangle$$
$$E_{xx} \neq \langle \psi_{yy} | \hat{H}_{yy} | \psi_{yy} \rangle + \langle \psi_{yy} | \hat{H}_{xx} - \hat{H}_{yy} | \psi_{yy} \rangle$$

Since just potentials differ from each other,

$$E_{xx} \neq E_{yy} + \int \rho(\boldsymbol{r})[V_{xx} - V_{yy}] d\boldsymbol{r} \tag{2.13}$$

Changing labels gives

$$E_{yy} \neq \langle \psi_{xx} | \hat{H}_{yy} | \psi_{xx} \rangle$$
$$E_{yy} \neq \langle \psi_{xx} | \hat{H}_{xx} | \psi_{xx} \rangle + \langle \psi_{xx} | \hat{H}_{yy} - \hat{H}_{xx} | \psi_{xx} \rangle$$
$$E_{yy} \neq E_{xx} + \int \rho(\boldsymbol{r})[V_{yy} - V_{xx}] d\boldsymbol{r} \tag{2.14}$$

Addition of 2.13 and 2.14 equations concludes in $E_{xx} + E_{yy} \neq E_{xx} + E_{yy}$. This result is mathematically wrong. So, two different potentials can not lead to same

density, $\rho(\boldsymbol{r})$.

The second theorem of Hohenberg Kohn states that a universal functional of density, $E[\rho]$, can be defined for energy. The global minimum of this functional gives the exact ground state of the system, and the density, $\rho(\boldsymbol{r})$, leading to the minimum value of the functional, refers to the exact ground state density, $\rho_o(\boldsymbol{r})$. The proof is as follows: the first theorem of Hohenberg-Kohn proves that the density, $\rho(\boldsymbol{r})$, determines the potential, $V(\boldsymbol{r})$. We already know from quantum mechanics that potential determines the Hamiltonian, the Hamiltonian determines the ground state wavefunctions, and the ground state wavefunctions determines the ground state density. As a result, every observable can be

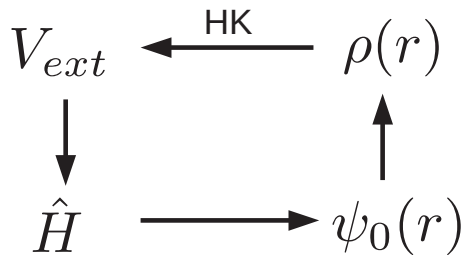

written as a functional of the ground state density.

$$F[\rho(\boldsymbol{r})] \;=\; \langle\, \psi \,|\hat{F}|\, \psi \,\rangle \tag{2.15}$$

Variational principle asserts that the total energy of the ground state can be found by minimizing the energy functional with respect to its density, $\rho(\boldsymbol{r})$ [26].

These theorems demonstrate that electronic density, rather than individual wavefunctions, can be used as the starting point. Why are the results of Hohenberg-Kohn theorems so important? The first thing is the computational time saving. Now, we are dealing with three spatial variables instead of 3N variables. Besides, wavefuncitons are not directly observable. On the contrary, density can be measured by experimental methods.

Although, Hohenberg-Kohn asserted two powerful theorems, they did not offer any prescription to apply their theorems in reality. But, Kohn-Sham did. In order to explain Kohn-Sham equations, it is required to restate the Hamiltonian here,

$$\hat{H} = K_{ee} + V_{Ie} + V_{ee} + V_{ex} \tag{2.16}$$

The kinetic energy term, K_{II}, and the nuclear potential term, V_{II} are absence under favour of the Born-Oppenheimer approximation. In order to write energy as a function of density as stated in the second theorem of Hohenberg-Kohn

$$\begin{aligned} E &= \langle\psi|\hat{H}|\psi\rangle \\ E &= \langle\psi|K_{ee}|\psi\rangle + \langle\psi|V_{Ie}|\psi\rangle + \langle\psi|V_{ee}|\psi\rangle + \langle\psi|V_{ex}|\psi\rangle \end{aligned}$$

Since both the nuclei-electron interaction term, V_{Ie}, and the electron-electron interaction term, V_{ee}, do not contain any derivatives or complexities, the wavefunction and its conjugate can be gathered under a common norm square, and to conclude

$$\langle V_{Ie}\rangle = -\sum_{I}^{Ne}\int \rho(\boldsymbol{r})V_{Ie}(\boldsymbol{r})d\boldsymbol{r} \tag{2.17}$$

The Hartree potential, equation 2.8, defines electron-electron interaction and its expectation values is

$$\langle V_{ee}\rangle = \frac{1}{2}\int\int d\boldsymbol{r}'d\boldsymbol{r}\frac{\rho(\boldsymbol{r}')\rho(\boldsymbol{r})}{|\boldsymbol{r}-\boldsymbol{r}'|} \tag{2.18}$$

However, in the case of both the exchange term and kinetic energy term, collection of wavefunction and its conjugate under a common norm square is impossible.

$$\langle V_{ex}\rangle = -\frac{1}{2}\sum_{i,j}^{N}\int\int \psi_i^*(\boldsymbol{r})\psi_j^*(\boldsymbol{r}')\frac{1}{|\boldsymbol{r}-\boldsymbol{r}'|}\psi_i(\boldsymbol{r})\psi_j(\boldsymbol{r}')d\boldsymbol{r}'d\boldsymbol{r} \tag{2.19}$$

$$\langle K_{ee}\rangle = -\frac{1}{2}\int d\boldsymbol{r}\ \psi^*(\boldsymbol{r})\ \bigtriangledown^2\ \psi(\boldsymbol{r}) \tag{2.20}$$

In order to handle the problem in kinetic energy term, assume that density is defined as the sum of norm squares of single-particle orbitals, called the Kohn-Sham orbitals, $\Theta_n(\boldsymbol{r})$.

$$\rho(\boldsymbol{r}) = \sum_{n}^{Ne}|\Theta_n(\boldsymbol{r})|^2 \tag{2.21}$$

Under favour of this assumption, it is now possible to consider the kinetic energy as a collection of individual kinetic energies of the Kohn-Sham orbitals. However, the consequent kinetic energy shall be different from the real kinetic energy. This difference is known as correlation.

Within Kohn-Sham approach, the ground state energy functional in the form

$$E_{ks} = K_s[\rho] + \int d\boldsymbol{r} V_{ext}(\boldsymbol{r})\rho(\boldsymbol{r}) + E_{ee}[\rho] + E_{xc}[\rho] \tag{2.22}$$

can be written where $V_{ext}(\boldsymbol{r})$ refers to the external potential due to the nuclei and any other external fields, respectively [23]. Now, the Hamiltonian can be divided into two parts

$$E_{KS}[\rho] = E_{known}[\rho] + E_{xc}[\rho] \tag{2.23}$$

where E_{known} is a collection of terms that can be determined exactly and E_{xc} is everything else, which includes exchange-correlation effects. In order to get the Kohn-Sham equations, one must derive the equation 2.23 with respect to density according to the second theorem of Hohenberg-Kohn. In case of kinetic energy, derivation with respect to density is impossible, instead it can be derived with respect to wavefunction conjugate, $\psi^*(\boldsymbol{r})$.

$$\frac{\delta E_{KS}}{\delta \Theta_i^*(\boldsymbol{r})} = \frac{\delta K_S}{\delta \Theta_i^*(\boldsymbol{r})} + \left[\frac{\delta E_{ext}}{\delta \rho(\boldsymbol{r})} + \frac{\delta E_{ee}}{\delta \rho(\boldsymbol{r})} + \frac{\delta E_{xc}}{\delta \rho(\boldsymbol{r})}\right] \frac{\delta \rho(\boldsymbol{r})}{\delta \Theta_i^*(\boldsymbol{r})} = 0 \tag{2.24}$$

With the Kohn-Sham equations, many particle system can be described in terms of single-particle orbitals

$$\left[-\frac{1}{2}\bigtriangledown^2 + V_{eff}\right]\Theta_i(\boldsymbol{r}) = \epsilon_i \Theta_i(\boldsymbol{r}) \tag{2.25}$$

with the important difference that V_{eff} is the sum of $V_{Hartree}$, V_{xc}, and V_{ext}. The exchange-correlation term contains all the complex many-body interactions, and it can not be handled easily. There are approximations to tackle exchange-correlation. The most commonly used one is local density approximation (LDA). And others are called generalized gradient approximation (GGA), exact exchange functionals, hybrid functionals and, LDA+U. DFT is still an subject of investigation.

DFT method has a very huge range of applications , and is a very efficient method to predict electronegativity, chemical potential, hardness, and chemical property[27, 28]. Even optical properties can be determined by using the time-dependent DFT. Still there are limitations. Calculations of large, complex systems such as biosystems, nanostructures, clusters, and nanoreactors are impossible with ab-initio methods, which do not include any experimental parameters. Since DFT does not contain empirical parameters, which come from experimental data, it is an ab-initio method.

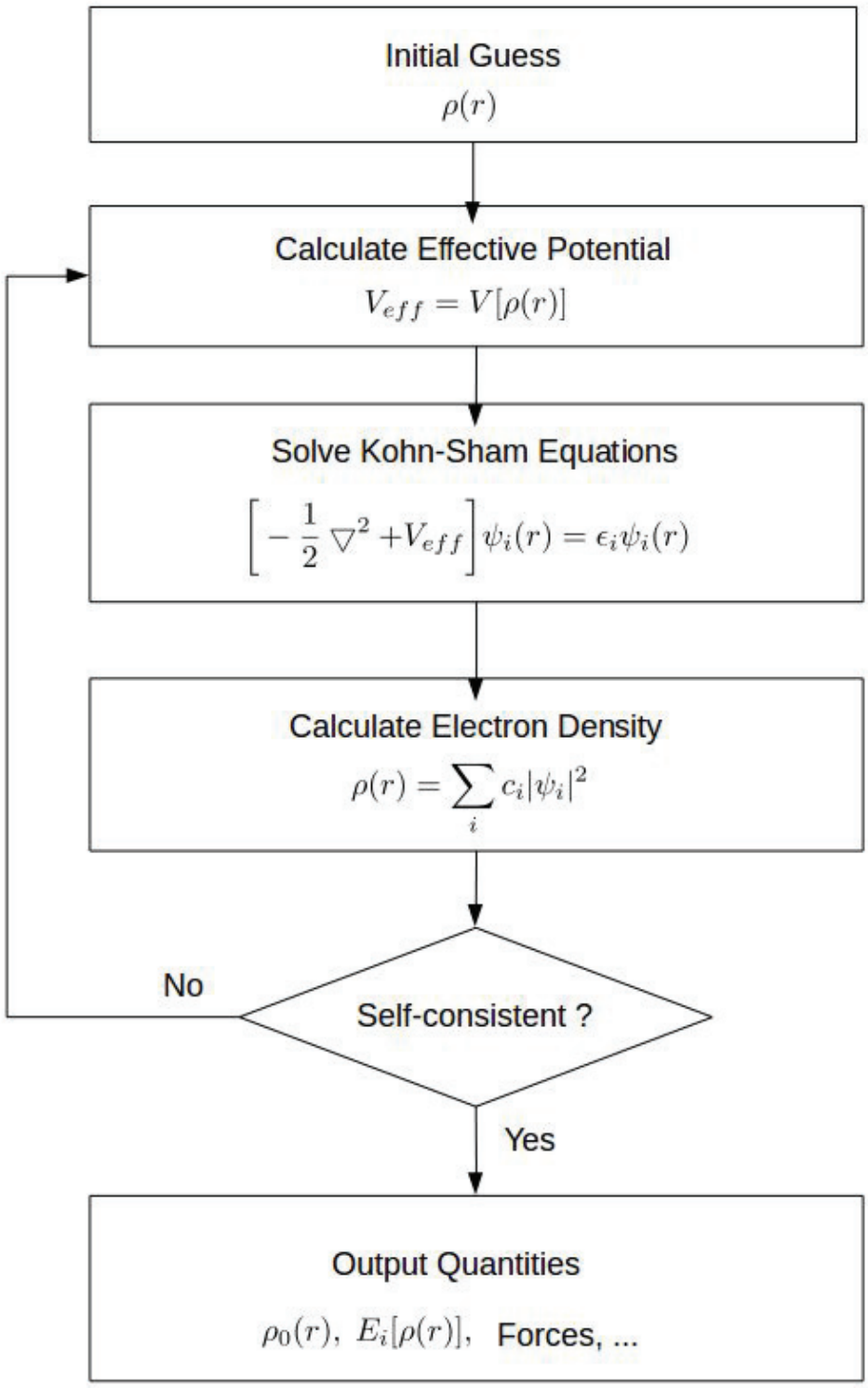

Figure 2.1. The self-consistent loop for solution of Kohn-Sham equations is represented as a schema. The figure is adapted from the reference [23]

2.2. Density Functional Tight Binding Theory

Density functional tight binding method (DFTB) is a tight binding method in which parameters are determined by DFT calculations of a few molecules. DFTB is not an ab-initio method as opposed to DFT, even though parameters are not derived from experimental data.

The simplest description of the tight binding method is to build a Hamiltonian matrix whose elements depend on the spatial parameters. The tight binding method assumes that electrons are tightly bound to the atom which they belong to. The tight binding method takes atomic-like orbitals as the basis set. In the tight binding method, total energy is divided into two components

$$E = E_{bnd} \; + \; E_{rep} \tag{2.26}$$

where E_{bnd} describes the energies of occupied orbitals, and E_{rep} describes the repulsive contribution. In order to use DFT as basis for a tight binding method, electronic density is described by

$$\rho(\boldsymbol{r}) = \rho_0(\boldsymbol{r}) + \delta\rho(\boldsymbol{r}) \tag{2.27}$$

Inserting the equation 2.27 into the equation 2.23 and writing it explicitly

$$\begin{aligned} E[\rho_0 + \delta\rho] = \sum_i^N n_i \left\langle \psi_i \right| -\frac{1}{2}\bigtriangledown^2 + V_{ext}(\boldsymbol{r}) + \int \frac{\rho_0'(\boldsymbol{r})}{|\boldsymbol{r}-\boldsymbol{r}'|} d\boldsymbol{r}' + V_{xc}[\rho_0] \left| \psi_i \right\rangle \\ - \frac{1}{2}\int\int \frac{\rho_0'(\rho_0+\delta\rho)}{|\boldsymbol{r}-\boldsymbol{r}'|} d\boldsymbol{r}' d\boldsymbol{r} - \int V_{xc}[\rho_0](\rho_0+\delta\rho) d\boldsymbol{r} \\ + \frac{1}{2}\int\int \frac{\delta\rho'(\rho_0+\delta\rho)}{|\boldsymbol{r}-\boldsymbol{r}'|} d\boldsymbol{r}' d\boldsymbol{r} + E_{xc}[\rho_0+\delta\rho] + E_{II} \end{aligned} \tag{2.28}$$

where $\rho_0' = \rho_0(\boldsymbol{r}')$, and $\delta\rho_0' = \delta\rho_0(\boldsymbol{r}')$. In this equation, E_{II} term describes nuclei-nuclei repulsion. The Taylor expansion of the exchange-correlation term, $E_{xc}[\rho_0 + \delta\rho]$, up to the second-order is

$$E_{xc}[\rho_0+\delta\rho] = E_{xc}[\rho_0] + \int \left.\frac{\delta E_{xc}}{\delta\rho}\right|_{\rho_0} \delta\rho d\boldsymbol{r} + \frac{1}{2}\int\int \left.\frac{\delta^2 E_{xc}}{\delta\rho\delta\rho_0'}\right|_{\rho_0} \delta\rho\delta\rho_0' d\boldsymbol{r} d\boldsymbol{r}' \tag{2.29}$$

Substition of the equation 2.29 into the equation 2.28 gives

$$E = \sum_i^N n_i \left\langle \psi_i \right| -\frac{1}{2}\bigtriangledown^2 + V_{ext}(\boldsymbol{r}) + \int \frac{\rho_0'}{|\boldsymbol{r}-\boldsymbol{r}'|} d\boldsymbol{r}' + V_{xc}[\rho_0] \left| \psi_i \right\rangle$$
$$- \frac{1}{2}\int\int \frac{\rho_0'\rho_0}{|\boldsymbol{r}-\boldsymbol{r}'|} d\boldsymbol{r}d\boldsymbol{r}' + E_{xc}[\rho_0] - \int v_{xc}[\rho_0]\rho_0 d\boldsymbol{r} + E_{II}$$
$$+ \frac{1}{2}\int\int \left(\frac{\delta\rho\delta\rho'}{|\boldsymbol{r}-\boldsymbol{r}'|} + \frac{\delta^2 E_{xc}}{\delta\rho\delta\rho'}\bigg|_{\rho_0} \right) d\boldsymbol{r}d\boldsymbol{r}' \tag{2.30}$$

where $(\delta E_{xc}/\delta\rho)_{\rho_0} = V_{xc}[\rho]$ is defined in brief. From the equation 2.30, one can divide energy into the E_{bnd} and the E_{rep} terms of the equation 2.26.

$$E_{bnd} = \sum_i^N n_i \left\langle \psi_i \right| -\frac{1}{2}\bigtriangledown^2 + V_{ext}(\boldsymbol{r}) + \int \frac{\rho_0'(\boldsymbol{r})}{|\boldsymbol{r}-\boldsymbol{r}'|} d\boldsymbol{r}' + V_{xc}[\rho_0] \left| \psi_i \right\rangle \tag{2.31}$$

$$E_{rep} = -\frac{1}{2}\int\int \frac{\rho_0'\rho_0}{|\boldsymbol{r}-\boldsymbol{r}'|} d\boldsymbol{r}d\boldsymbol{r}' + E_{xc}[\rho_0] - \int v_{xc}[\rho_0]\rho_0 d\boldsymbol{r} + E_{II} \tag{2.32}$$

The term, which represents corrections, depends on the fluctuations in the density, is called second-order correction term.

$$E_{2nd}[\rho_0, \delta\rho] = \frac{1}{2}\int\int \left(\frac{\delta\rho\delta\rho'}{|\boldsymbol{r}-\boldsymbol{r}'|} + \frac{\delta^2 E_{xc}}{\delta\rho\delta\rho'}\bigg|_{\rho_0} \right) d\boldsymbol{r}d\boldsymbol{r}' \tag{2.33}$$

In the standart DFTB model, which is solved without self-consistency, this term is neglected. The non-self-consistent solution of DFTB is convenient to determine properties of homonuclear systems. However, the second-order correction term can not be negligible in the systems where chemical bonds are sensitive to the charge balance such as heteronuclear molecules and polar semiconductors[29]. In this case, the self-consistent charge correction scheme is a more proper way to study these systems. [30]

Implementation of DFTB method is achieved by using DFTB+ software package. The structure's geometries are optimized by using the conjugate gradient algorithm. Optimizations stop when the force component with the maximal value drops below 0.02 eV/Angstrom. Lattice parameters are optimized to yield the minimum energy. The DFTB

Hamiltionian with self-consistent charge calculation(SCC) is solved. The SCC tolerance is set to 1.0e-7 Hartree. Mixer type for mixing charges in an SCC calculation is Broyden with 1.5 mixing parameter.

2.3. Hellman-Feynman Theorem

Once the ground state structure has been reached, molecular forces can be calculated by using the Hellmann-Feynman theorem. The Hellman-Feynman theorem states

$$\frac{dE}{d\lambda} = \left\langle \psi(\lambda) \middle| \frac{dH}{d\lambda} \middle| \psi(\lambda) \right\rangle \tag{2.34}$$

The most widely used application of the Hellmann-Feynman theorem is the calculation of molecular forces since

$$\boldsymbol{F}_{i\alpha} = -\frac{\partial E}{\partial \boldsymbol{R}_{i\alpha}} = -\left\langle \psi \middle| \frac{\partial H}{\partial \boldsymbol{R}_{i\alpha}} \middle| \psi \right\rangle \tag{2.35}$$

This is a very important and practical result since fluctuations of wavefunctions can be ignored, thus changes in the Hamiltonian are calculated exclusively[31]. Since only the term V_{ext} and E_{II} depend on atomic coordinates,

$$\boldsymbol{F}_{i\alpha} = -\int d\boldsymbol{r}\rho(\boldsymbol{r})\frac{\partial V_{ext}}{\partial \boldsymbol{R}_{i\alpha}} - \frac{\partial E_{II}}{\partial \boldsymbol{R}_{i\alpha}} \tag{2.36}$$

2.4. Finite Displacements Method

In order to obtain force constants, the finite differences method, in the present case the finite displacements method, is used. Firstly, geometries are optimized by using the DFTB method. Then one atom from the low energetic configuration is dislodged each time. The number of new configurations that are generated by dislodging one atom depends on the symmetries of the original low energetic configuration. The forces of these new configurations are calculated by using the DFTB method. After the calculations of

forces, finite differences method is applied in order to gain the force constants from the forces [32].

$$\boldsymbol{C}_{\alpha\beta}(jl, j'l') \simeq -\frac{\boldsymbol{F}_{\beta}(j'l'; \Delta\boldsymbol{r}_{\alpha}(jl)) - \boldsymbol{F}_{\beta}(j'l')}{\Delta\boldsymbol{r}_{\alpha}(jl)} \tag{2.37}$$

In this equation, $\Delta\boldsymbol{r}_{\alpha}(jl)$ represents finite displacement of dislodged atom and $\boldsymbol{F}_{\beta}(j'l'; \Delta\boldsymbol{r}_{\alpha}(jl))$ is the force on the dislodged atom. $\boldsymbol{F}_{\beta}(j'l')$ is calculated from the equilibrium position of the dislodged atom and is usually zero.

The software package, named as Phonopy, is used to apply the finite differences method. Phonopy takes optimized geometry structure as input, and creates supercell structures with displecements from optimized geometry. Phonopy also creates the perfect supercell structure without displacements. Phonopy does not calculate forces. In order to calculate forces, one can use his/her own favorite calculator such as VASP, Siesta, etc. In this research, DFTB+ package is used. Once the forces are calculated, the force constants are calculated with the equation 2.37 by using Phonopy "–fc" tag. In addition, the thermal properties (density of states, band structure, etc) can be determined by using Phonopy. [33]

2.5. Zero Force Condition

Interatomic potentials are described by considering two-body interactions, $U(\boldsymbol{R})$, where $\boldsymbol{R}$ is interatomic distance between a pair of atoms. Because the standard two-body interatomic potential curve exhibits asymmetric behaviour, $U(\boldsymbol{R})$ can be expanded as Taylor series around its minimum

$$U = U(\boldsymbol{R}_0) + \left(\frac{\partial U}{\partial R}\right)_0 x + \frac{1}{2}\left(\frac{\partial^2 U}{\partial R^2}\right)_0 x^2 + ... \tag{2.38}$$

The zeroth-order term of the series is constant as well as insignificant. The first-order term must vanish since it identifies a force, and total force acting on an atom must be zero in the equilibrium configuration. The terms with order that are higher than the second-order are ignored since just non-interacting phonons are considered due to the fact that ballistic transport dominates the regime which is under interest . In the harmonic approximation, the quadratic term is taken into consideration, and it defines an interatomic force

constant [7]. Furthermore, zero force condition reflects to the matrix of force constants as

$$\boldsymbol{C}_{\alpha\beta}(jl, jl) = -\sum_{j'l' \neq jl} \boldsymbol{C}_{\alpha\beta}(jl, j'l') \tag{2.39}$$

The force constants, $\boldsymbol{C}_{\alpha\beta}(jl, jl)$, are called on-site terms .

2.6. Atomistic Green's Function

Density functional tight binding method is combined with atomistic Green's function method in order to characterize phonon transport characteristics. Atomistic Green's function method(AGF) is an efficent method to determine the transport properties of molecular junctions.

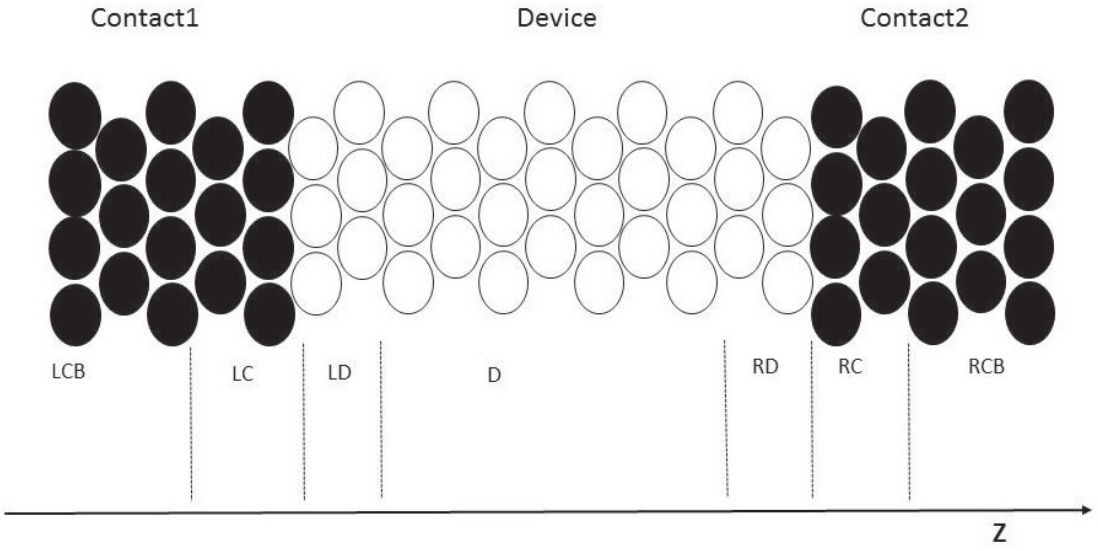

Figure 2.2. The general set-up for atomistic Green's function. The dark atoms located on the left represent the left contact bulk region, the white atoms represent the region of the device, the dark atoms located on the right represent the right contact bulk region. The figure is adapted from the reference [34].

Molecular transport junctions, one of the building blocks of nano-scale devices, are the constituents in which a single molecule is placed between two electrodes but in phononic cases, thermal reservoirs are placed instead of the electrodes [35, 36]. The gen-

eral structure for Green's function method is illustrated in the figure 2.2. The construction consists of three regimes: left contact bulk region (LCB), right contact bulk region (RCB) and, device. LCB and RCB are two semi-infinite thermal reservoirs.

The AGF method starts with constructing the dynamical matrix of the system under interest. The description of dynamical matrix is

$$\hat{D} = \{\hat{D}_{pq}\} = \frac{1}{M_p M_q} \begin{cases} -\dfrac{\partial^2 U}{\partial u_p \partial u_q}, & \text{if} \quad p \neq q \\ -\displaystyle\sum_{m \neq q} \dfrac{\partial^2 U}{\partial u_q \partial u_m}, & \text{if} \quad p = q \end{cases} \tag{2.40}$$

where u_p and u_q refer to any atomic degree of freedom (i.e. displacements), and U indicates the total interatomic potential. M_p and M_q are atomic masses associated with degrees of freedom u_p and u_q, respectively. Here, just harmonic non-interacting phonons are considered. Anharmonicity (nonlinearism) can be neglected due to the fact that the regime in which the ballistic transport is dominant, is under interest.

The next step of the AGF method is to calculate free Green's functions of the reservoirs. The dynamical equation for the system is

$$((w^2 + \delta i)\mathbb{1} - \hat{D})\hat{u} = \mathbb{1} \tag{2.41}$$

where u is a coloumn vector that consists vibrational degrees of freedom and δ is an arbitrary constant. The non-contact Green's function is

$$g = ((w^2 + \delta i)\mathbb{1} - \hat{D})^{-1} \tag{2.42}$$

After connections set between reservoirs and device, the following matrix occurs

$$\begin{bmatrix} (w^2 + \delta i)\mathbb{1} - \hat{D}_L & -\tau_L^\dagger & 0 \\ -\tau_L & (w^2 + \delta i)\mathbb{1} - \hat{D}_d & -\tau_R \\ 0 & -\tau_R^\dagger & (w^2 + \delta i)\mathbb{1} - \hat{D}_R \end{bmatrix} \begin{Bmatrix} g_{LD} \\ G_D \\ g_{RD} \end{Bmatrix} = 0 \tag{2.43}$$

where τ_L and τ_R are interaction matrices between the device and the left reservoir and between device and right reservoir, respectively. The terms, $g_{LD(RD)}$, represent the Green's functions of reservoirs including the changes when the connections are established. When

multiplication is achieved,

$$((w^2 + \delta i)\mathbb{1} - \hat{D}_L)\ g_{LD} - \tau_L^\dagger G_D = 0 \tag{2.44}$$

$$-\tau_L\ g_{LD} + ((w^2 + \delta i)\mathbb{1} - \hat{D}_D)G_D - \tau_R\ g_{RD} = \mathbb{1} \tag{2.45}$$

$$((w^2 + \delta i)\mathbb{1} - \hat{D}_R)\ g_{RD} - \tau_R^\dagger G_D = 0 \tag{2.46}$$

Since $((w^2 + \delta i)\mathbb{1} - \hat{D}_{L(R)}) = g_{L(R)}{-}1$, the equations 2.44 and 2.46 become

$$g_{LD} = g_L \tau_L^\dagger G_D \tag{2.47}$$

$$g_{RD} = g_R \tau_R^\dagger G_D \tag{2.48}$$

Inserting the equations 2.47 and 2.48 into the the equation 2.45 concludes the Green's function of the device

$$G_D = \left[(w^2 + \delta i)\mathbb{1} - D_d\ -\ \tau_L g_L \tau_L^\dagger\ -\ \tau_R g_R \tau_R^\dagger\right]^{-1} \tag{2.49}$$

where $\mathbb{1}$ is the unity matrix.

The broadening terms are imaginary components of self-energy terms, Σ. Self-energy terms are calculated from the Green's function of the reservoirs and the interaction matrices

$$\Gamma^{L(R)} = -2Im(\Sigma^{L(R)}) = -2Im(\ \tau_{L(R)} g_{L(R)} \tau_{L(R)}^\dagger\ ) \tag{2.50}$$

Transmission function is

$$\Xi(w) = \textit{Trace}[\Gamma_L G_D \Gamma_R G_D^\dagger] = \textit{Trace}[\Gamma_R G_D \Gamma_L G_D^\dagger] \tag{2.51}$$

since at the steady state the total energy flux is independent of the direction. The heat flux in the Landauer form is

$$J = \frac{1}{2\pi} \int dw\ \hbar w\ \Xi(w)\ [f_L(w,T) - f_R(w,T)] \tag{2.52}$$

where $f_{L(R)}(w,T)$ are the Bose-Einstein distribution functions.

Finally, conductance is

$$\kappa = \frac{J}{\Delta T} \tag{2.53}$$

Assuming that $\Delta T \to 0$, namely equilibrium transport condition, then conductance become

$$\kappa = \frac{1}{2\pi} \int dw\ \hbar w\ \Xi(w)\ \frac{\partial f}{\partial T}; \tag{2.54}$$

since

$$\frac{f_L(T + \frac{\Delta T}{2}) - f_R(T - \frac{\Delta T}{2})}{\Delta T} = \frac{\partial f}{\partial T} \tag{2.55}$$

2.7. Generic Reservoir

Consider a one-dimensional linear chain with the first nearest neighbour interaction. The relationship between its frequency, ω, and its wavevector, $\boldsymbol{k}$, is

$$\omega = \sqrt{\frac{4\boldsymbol{C}}{M}} \sin\left(\frac{\boldsymbol{k}a}{2}\right) \qquad and \qquad \omega_{max} = \sqrt{\frac{4\boldsymbol{C}}{M}} \tag{2.56}$$

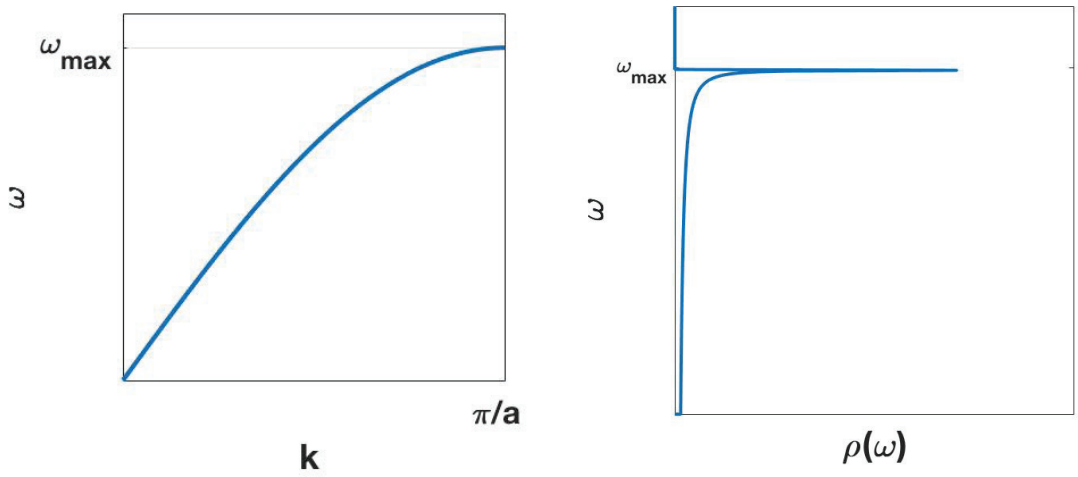

Figure 2.3. Phonon dispersion relation (left) and phononic density of states (right) of a one-dimensional monoatomic linear chain

The group velocity of phonons, which are propagating through the one-dimensional chain, is described as

$$\frac{d\omega}{d\boldsymbol{k}} = \sqrt{\frac{4\boldsymbol{C}}{M}} \frac{a}{2} \cos\left(\frac{\boldsymbol{k}a}{2}\right) \tag{2.57}$$

and it describes transmission of a phonon wave packet. The group velocity at low values of wavevector gives sound velocity, which gives the speed of acoustic phonons.

$$\lim_{\boldsymbol{k}\to 0} \frac{d\omega}{d\boldsymbol{k}} = \sqrt{\frac{4\boldsymbol{C}}{M}}\frac{a}{2} = v_g = v_s \tag{2.58}$$

The tight binding dynamical matrix operator of a semi-infinite linear chain is

$$D_0 = \begin{pmatrix} \alpha & -\gamma & 0 & 0 & ... \\ -\gamma & \alpha & -\gamma & 0 & \ddots \\ 0 & -\gamma & \alpha & -\gamma & \ddots \\ \vdots & \ddots & \ddots & \ddots & \ddots \end{pmatrix} \tag{2.59}$$

$$\text{where} \qquad \alpha = \frac{2\boldsymbol{C}}{M} \qquad \text{and} \qquad \gamma = \frac{\boldsymbol{C}}{M} = \frac{\alpha}{2} \tag{2.60}$$

Compensating the equations 2.58 and 2.60 gives $\alpha = v_s^2/a^2$. Once one knows the $\alpha \; and \; \gamma$, the Hamiltonian matrix can be constructed. The Green's function can be calculated analytically from the tight binding dynamical matrix elements as shown in W.Müller's work.[37]

$$g_{kl}^0 = -\frac{1}{\omega^2}\frac{\exp(i(k+l)\theta) - \exp(i(k-l)\theta)}{2i\sin(\theta)} \tag{2.61}$$

$$\text{where} \qquad t = \frac{(\omega^2 - \alpha)}{2\gamma} \qquad \text{and} \qquad \theta = \arccos(-t) \tag{2.62}$$

because the first atom of the chain, which is going to link to the molecule, is under interest, $k = l = 1$, and this condition reduces the equation 2.61

$$g_{11}^0 = -\frac{\hbar M}{\boldsymbol{C}}\exp(i\theta) \tag{2.63}$$

With this scheme, one can easily derive the Green's function of the reservoirs from their sound velocity without doing complex, time consuming optimization step, and calculation of forces step. The elements of the tight binding dynamic matrix of the semi-infinite chain are calculated by using sound velocity of carbon nanotubes. The on-site terms equal to $2v_s^2/a^2$, and the first-neighbour interaction terms equal to v_s^2/a^2. However, these steps are still requisite for molecules which are intended to be used as device. These

molecules have to be optimized and their matrix of force constants is determined by the methods explained in the previous sections. In order to connect the generic reservoirs to the molecule, each atom, which is located at the sides of the molecule where generic reservoirs are going to be bind to, is removed. The generic reservoirs are placed to these empty locations. While placing the reservoirs, care must be taken about the charge balance, which must be preserved. One atom from each reservoir is included to the force matrix of the molecule. In order to perform this, the corresponding elements of these removed atoms in the force matrix of the molecule are set to zero. After that, $M\alpha$ is inserted for on-site terms of the replaced atoms, and $-M\gamma$ is inserted for the terms which describe interactions between the replaced atoms and the atoms of the molecule linked to the reservoirs.

To make things clear, let's consider the benzene molecule. This toy model was applied to benzene molecule and results were investigated in depth. The first and twelfth hydrogen atoms (see the figure 2.4) are removed from both the molecule and its matrix of force constants . To reflect this effect to the matrix, substitution of corresponding elements with zero was carried out followed by replacement of previous zero values with appropriate values. Furthermore, $2Mv_s^2/a^2$, is inserted to $C_{(1,1)}$ and $C_{(12,12)}$. Mv_s^2/a^2, is inserted to $C_{(1,2)}$, $C_{(2,1)}$, $C_{(11,12)}$, $C_{(12,11)}$. By this substitution, the matrix of force constants of the benzene is ready for construction of dynamic matrix of device. Consequently, in order apply the atomistic Green's function method, all necessary information is known, thus thermal conductivity can be determined. Figure 2.5 shows the transmission and density of states of benzene, which are determined by virtue of generic reservoir.

The last thing, required to be defined, is a term, called switching effect:

$$SE = \frac{|\kappa_{trans} - \kappa_{cis}|}{\kappa_{trans}} x100 \tag{2.64}$$

The term gives information numerically how much isomeric changes affect the phononic conductivity. Switching effect is calculated from conductances of systems at 300K.

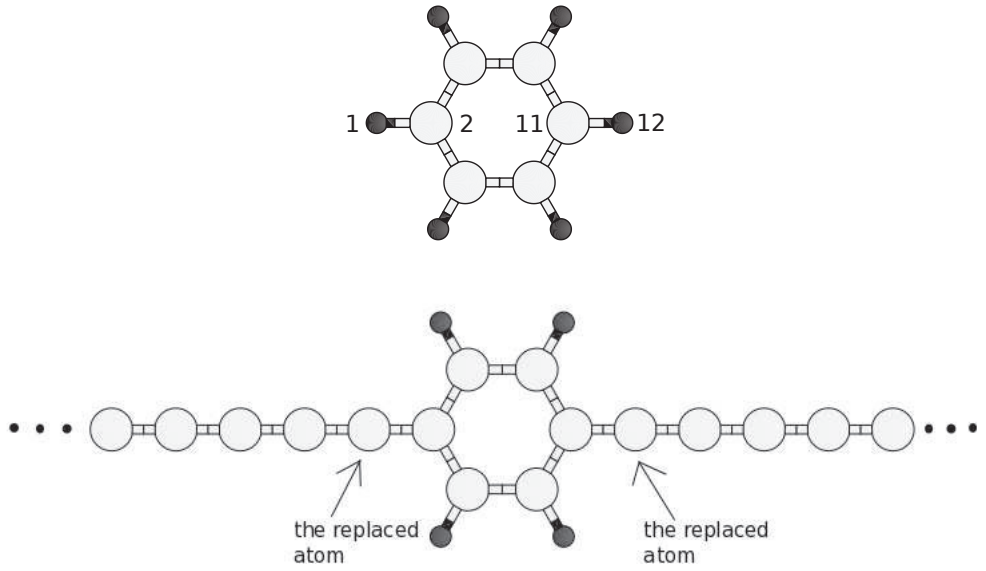

Figure 2.4. Illustrations of a free benzene molecule (top), and a connected benzene molecule with generic reservoirs (bottom). The first and twelfth hydrogen atoms are removed, and the generic reservoirs are placed to these empty locations.

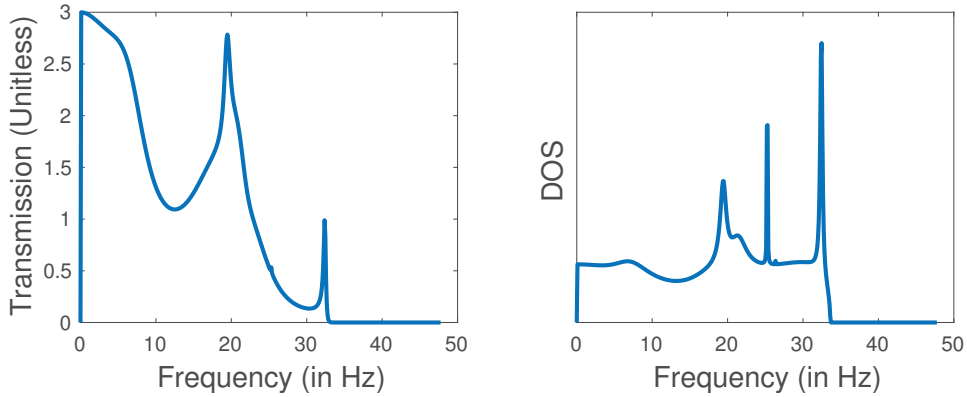

Figure 2.5. Transmission plot (left) and density of states plot (right) of benzene are illustrated. They are calculated within generic reservoir scheme.

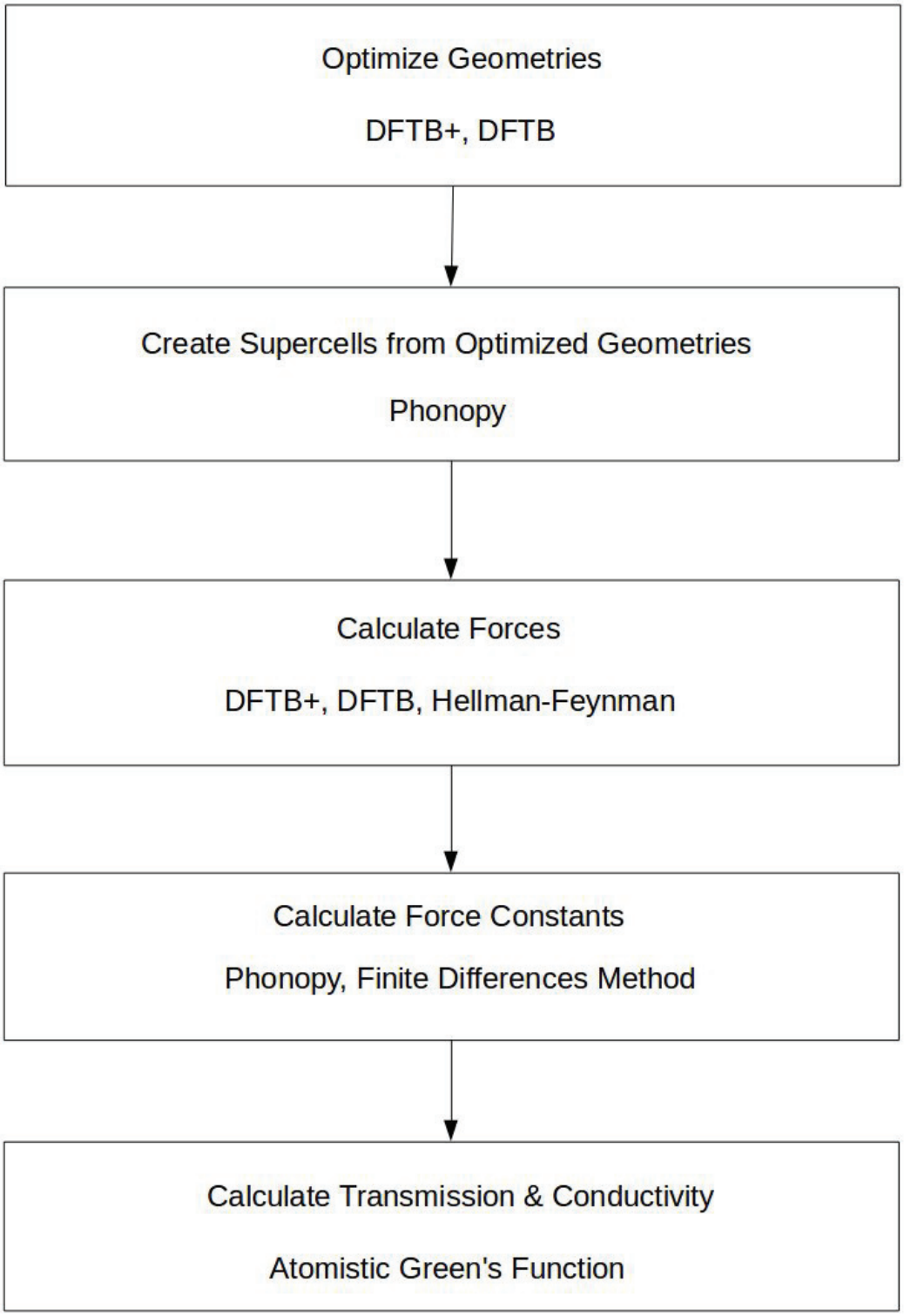

Figure 2.6. Alignment of methods

CHAPTER 3

SYSTEM SET-UP

3.1. Carbon nanotubes

A carbon nanotube is a carbon allotrope with a tube shape, which can be considered as a rolled sheet of graphene. Graphene is a two-dimensional hexagonal lattice of sp^2 hybridized carbon atoms while carbon nanotube is a one-dimensional tube. Carbon nanotubes attract considerable attention since they possess extraordinary properties. Due to the long mean free path, carbon nanotubes are ballistic conductors. Carbon nanotubes have high carrier concentration for electrons and holes because of the delocalized π-electrons donated by each atom. Graphene, diamond, and carbon nanotubes are very strong materials because of the double bond character arising from sp^2 hybridized carbon atoms. Due to the same reason, melting temperatures of carbon materials are high. In addition, cylindrical shape makes carbon nanotubes stronger than graphene. The Debye temperatures are high in carbon nanotubes as well as other carbon materials.

Electrical characteristics of carbon nanotubes can be altered between conducting and semiconducting states via structural design. These unique properties make carbon nanotubes promising candidates to build effective nanostructures. A great variety of applications of carbon nanotubes have come to light since their discovery in 1991. One of their extraordinary applications is that they can be used to construct aerospace devices, since carbon nanotubes are hard materials and have high melting temperatures [38]. Carbon nanotubes are still under interest in many scientific areas such as material science, electronics, mechanics, energy management, chemical processing, and many other fields.

Carbon nanotubes can possess a single outer wall or multiple walls (see the figure 3.1). Multiple walled carbon nanotubes are irrelevant to this study. However, single walled carbon nanotubes are used as thermal reservoirs. There are three different kinds of chiralities for a single walled carbon nanotube depending on its rolling vector (see the figure 3.2): zigzag, armchair, chiral. Single walled carbon nanotubes are identified by their rolling vector indices, (n, m). In this research, (5,5) armchair carbon nanotube and (9,0) zigzag carbon nanotube are used. The figure 3.3 illustrates the unit cells of carbon nanotubes which are used in this research.

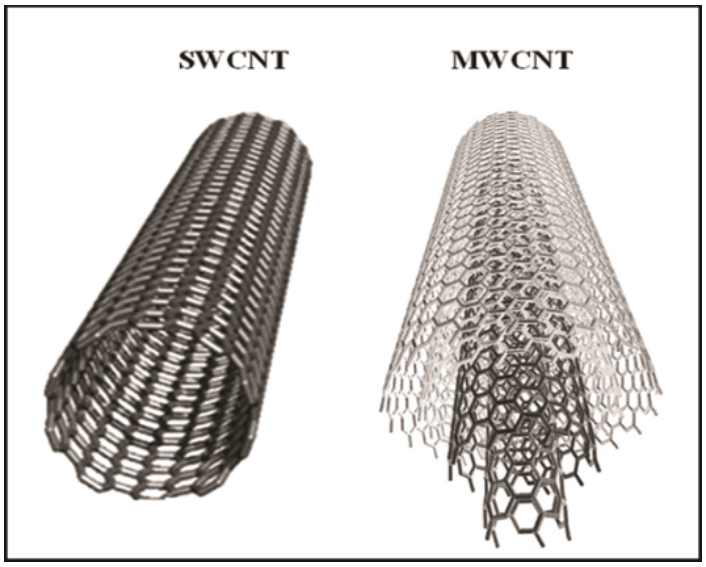

Figure 3.1. A single walled carbon nanotube (on the left), a multi walled carbon nanotube (on the right). The figure is adapted from the reference [39].

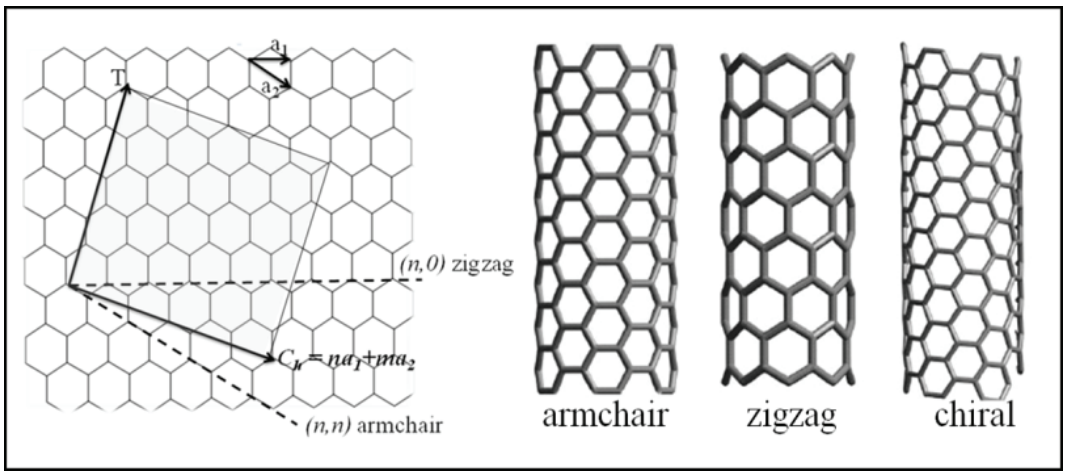

Figure 3.2. Figure of different chirality of a carbon nanotube. There are three different chiralities of a carbon nanotube depending on its rolling vector, C_k. The figure is adapted from the reference [39].

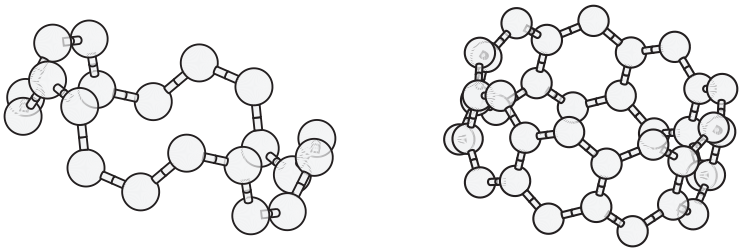

Figure 3.3. Figure of unit cells of (5,5) armchair carbon nanotube (left) and (9,0) zigzag carbon nanotube (right). The unit cell of a (5,5) armchair carbon nanotube consists of 20 carbon atoms, the unit cell of a (9,0) zigzag carbon nanotube consists of 36 carbon atoms.

3.2. Azobenzene

Azobenzene is a molecule which exhibits photoisomeric behaviour. When exposed to radiation, azobenzene changes its three-dimensional structure reversibly between its two isomeric states. The energy difference between the two isomeric states is 0.2 eV. The *trans* isomer is characterized by its planar structure, while benzene rings of the *cis* isomer are tilted with respect to each other. Especially, in electronics and photonics, this structural difference gives rise to potential applications to design devices whose particular properties can be controlled by light. The *trans* isomer of azobenzene have π-conjugation across the whole molecule, however, the ”v” shape of the *cis* isomer breaks this conjugation. This leads to significant changes in its electronic spectrum and gives the opportunitiy to construct very powerful electronic switches [40–42], diodes [43, 44], transistors [45, 46]. This π-conjugation also makes the *trans* isomers more stable than the *cis* isomers.

The most important reason of the difference between the vibrational spectrums of the isomers of azobenzene, which is seen in the figure 3.5, comes from the non-planarity of *cis* isomer. π-electrons are localized on the azo-group (central $N = N$ bond) instead of the whole molecule, as a result both double bond character of azo-group and the single bond character of adjent CN bonds are increased [47].

Azobenzene derivatives are also used as junction. 1,2-di([1,1’-biphenly]-4-yl) diazene and 1,2-di([1,1’:4’,1”-terphenly]-4-yl) diazene are called azobiphenly and azotriphenly in this research for abbreviation purposes (see figure 3.4). The prefix, (E)-, represents the *trans* conformation and the prefix, (Z)-, represents the *cis* conformation. Besides azobenzene, azobenzene derivatives are widely used in researches [41, 48]. The photoiso-

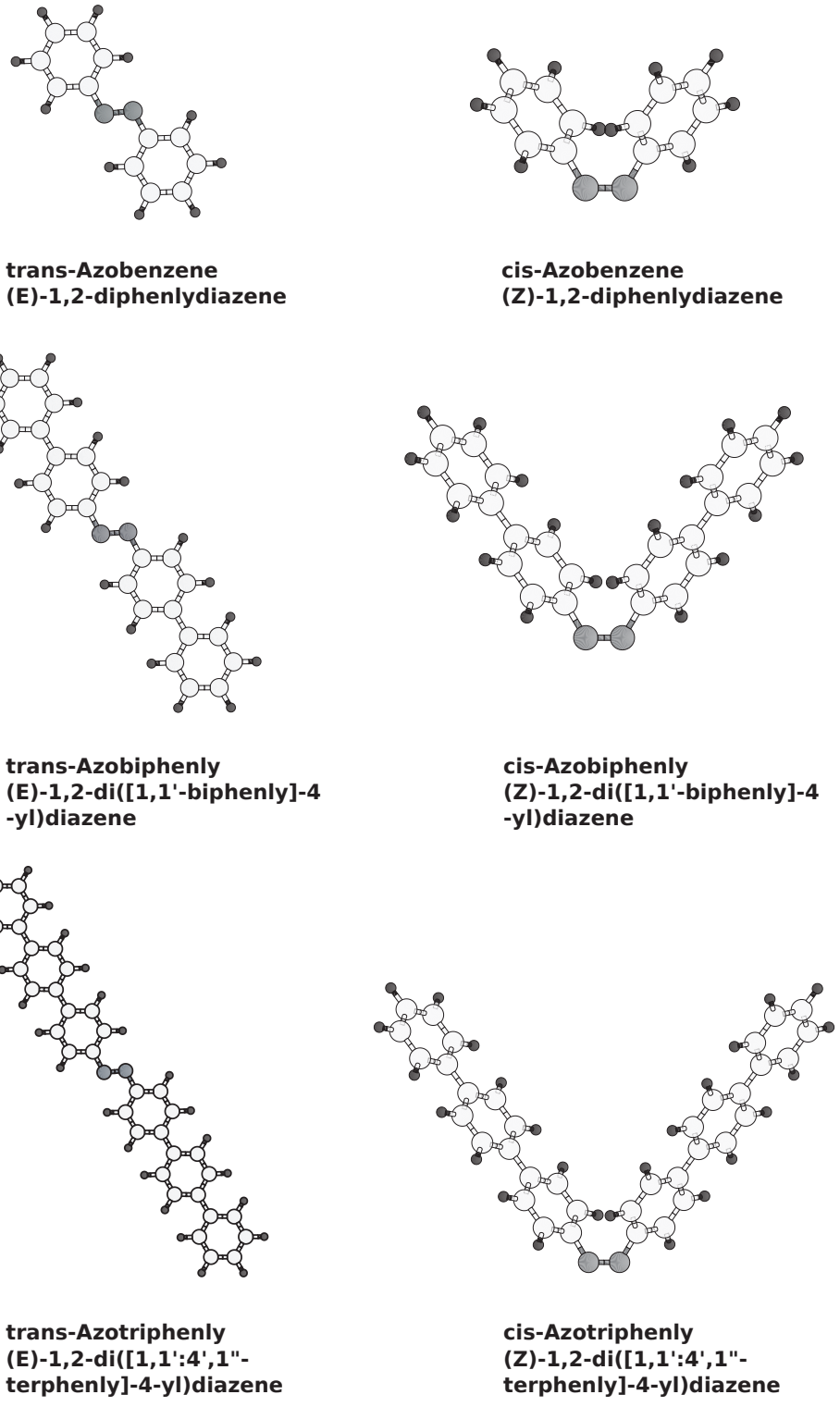

Figure 3.4. Illustration of isomers of azobenzene and its derivatives. Molecules on the left illustrate *trans* isomers, molecules on the right illustrate *cis* isomers.

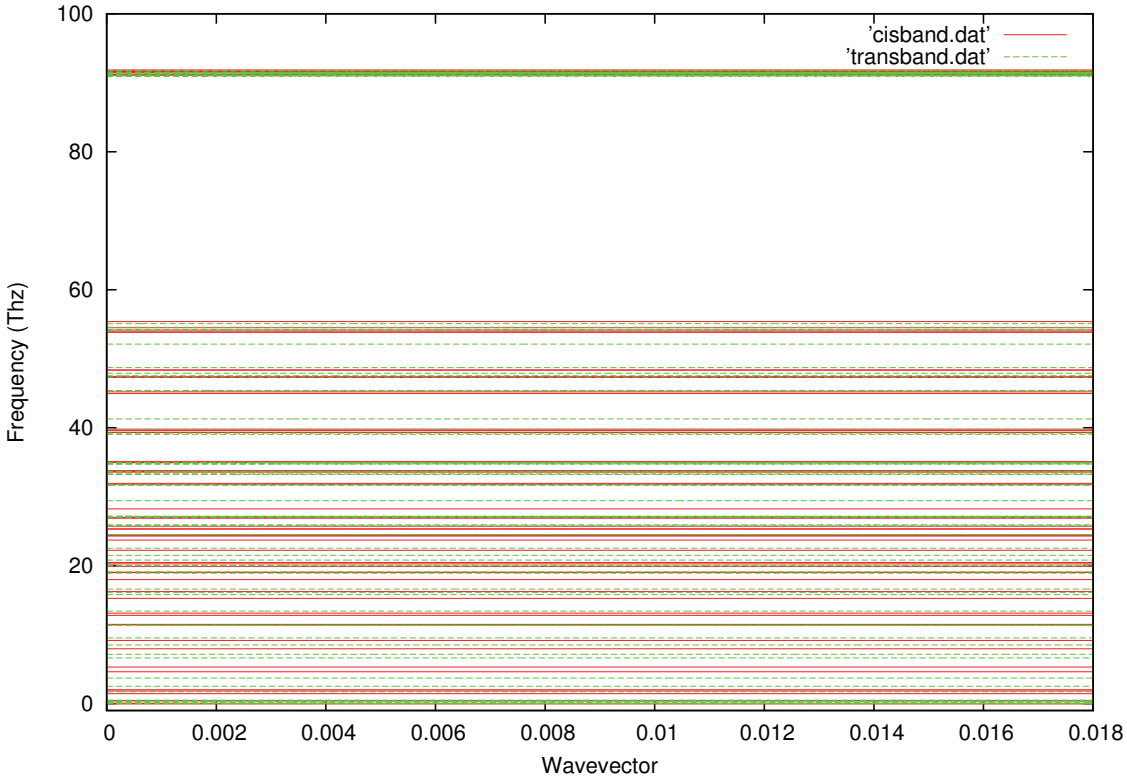

Figure 3.5. To see the difference betweeen vibrational spectrums of two isomers of azobenzene, each spectrum is plotted in the same figure. The red lines belong to the *cis* isomer of azobenzene while the green lines belong to the *trans* isomer of azobenzene.

merisation behaviour is also displayed by both azobiphenly and azotriphenly molecules. The energy difference between their isomers is approximately same with the energy difference between azobenzene isomers. Many characteristic properties are same for all. For *cis* isomer's dihedral angles, table 4.3 can be seen. The motivation in the usage of derivatives is the expectation of improving switching effect by extension of the molecules.

3.3. Molecular Junction

The figure 3.6 demonstrates the partition of our systems. A single azobenzene, or one of its derivatives is placed between two semi-infinite carbon nanotubes. A single azobenzene is placed between single walled five periodic cells (approximately 12.4971 angstroms) (5,5) armchair and five periodic cells (approximately 19.8 angstroms) (9,0) zigzag CNTs in order to construct the device. The hydrogen atoms at para positions of

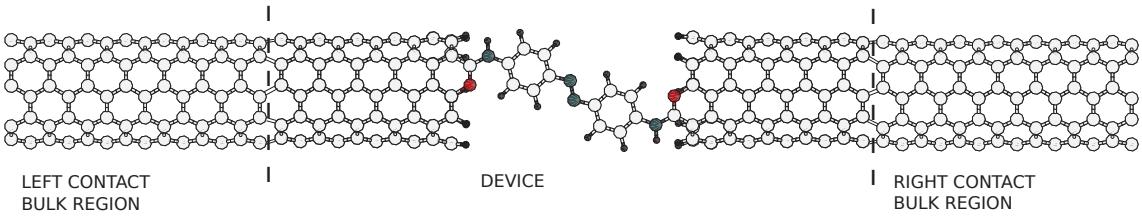

Figure 3.6. A schematic diagram of our system. The left and right contact bulk regions are two semi-infinite carbon nanotubes. The junction molecule is the *trans* isomer of azobenzene. The device includes five unit cells of carbon nanotubes from both left and right end.

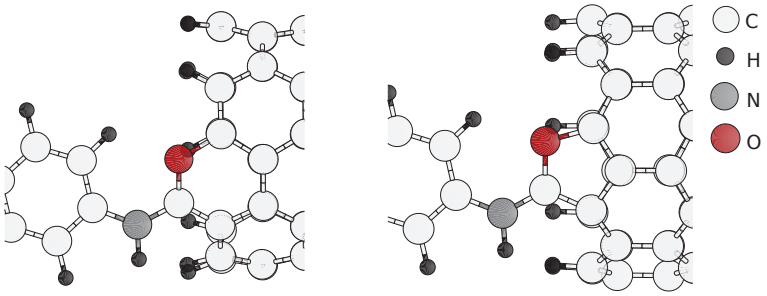

Figure 3.7. A close look to the geometry of junctions. The hexagone of armchair carbon nanotube which is completed with CO atoms of the $CONH$ linker is illustrated on the left. The heptagone of zigzag carbon nanotube which is completed with CO atoms of the $CONH$ linker is illustrated on the right.

azobenzene are removed, and $NHCO$ linker or $NH(CO)_2$ linker is placed. The arrangement of the linkers is important. The *cis* and *trans* isomers are able to transform to each other, only the separation of reservoirs is allowed to change. The incomplete hexagon of armchair carbon nanotube and the incomplete heptagon of zigzag carbon nanotube are completed with the oxygen and carbon atoms of the linkers. Their places must be the same in each condition. Figure 3.7 demonstrates the $NHCO$ linker case. Each carbon atom of CNTs on the linker's side with incomplete bonds are saturated with hydrogens. Three periodic cells (6.2653 angstroms) of the device's CNTs are fixed from both right end and left end. From both left and right end, three periodic cells (11.2258 Angstroms) of zigzag CNTs of device are fixed as well. Simulation window is large enough to avoid the self-interaction of the system. Device is contacted with LCB from left and RCB from right.

CHAPTER 4

NUMERICAL RESULTS

4.1. Structural analysis

Building of the constructions start with the relaxation of the unit cells of carbon nanotubes which are illustrated in the figure 3.3. Once relaxations of the unit cells are achieved, supercells are constructed from these unit cells in order not only to calculate the forces of reservoirs but also to construct contacts which are $1 \times 1 \times 5$ supercells of carbon nanotubes of devices. Furthermore, these contacts have perfect geometries. Molecules, which are intented to be used as junction, are placed between contacts as explained in the last section of the system set-up chapter. After the connection between contacts and molecules are established, structures are ready to be optimized in order to get low energetic configurations. The structures were optimized by using DFTB method, and to accomplish this, DFTB+ package was used. During optimizations, three periodic of carbon nanotubes from both left and right end of the device are fixed in order to preserve the periodicities of the simulation cells of devices. To accomplish this, contact's separations are changed exclusively, while molecules and the rest two periodic cells located at the molecule side of contacts are allowed to be relaxed. Figure 4.1 demonstrates an array of graphs which are the plotted energy versus contact's separation. The global minimum of these curves give the low energetic configurations. In each graph, the blue line stands for *cis* isomer, while the green line represents *trans* isomer. In each condition, the device in which the junction is constructed from *trans* isomer is more stable than the device in which the junction is constructed from *cis* isomer. The devices with *cis* isomeric junctions have a higher free energy than the devices with *trans* isomeric junctions. The one with the higher free energy is metastable. Between both states, it is a necessary condition of the energy barrier to be much larger than the thermal energy in order to avoid uncontrollable isomerization.

Some characteristic features of azobenzene and its derivatives change after connections are established. Energy differences between the isomers of free azobenzene, azobiphenly and, azotriphenly molecules are calculated as 0.18 eV, 0.202 eV, 0.203 eV, respectively. The largest numerical deviation in energy differences occurs when azobenzene is connected with armchair CNT and its value is approximately 0.1 eV. Because the

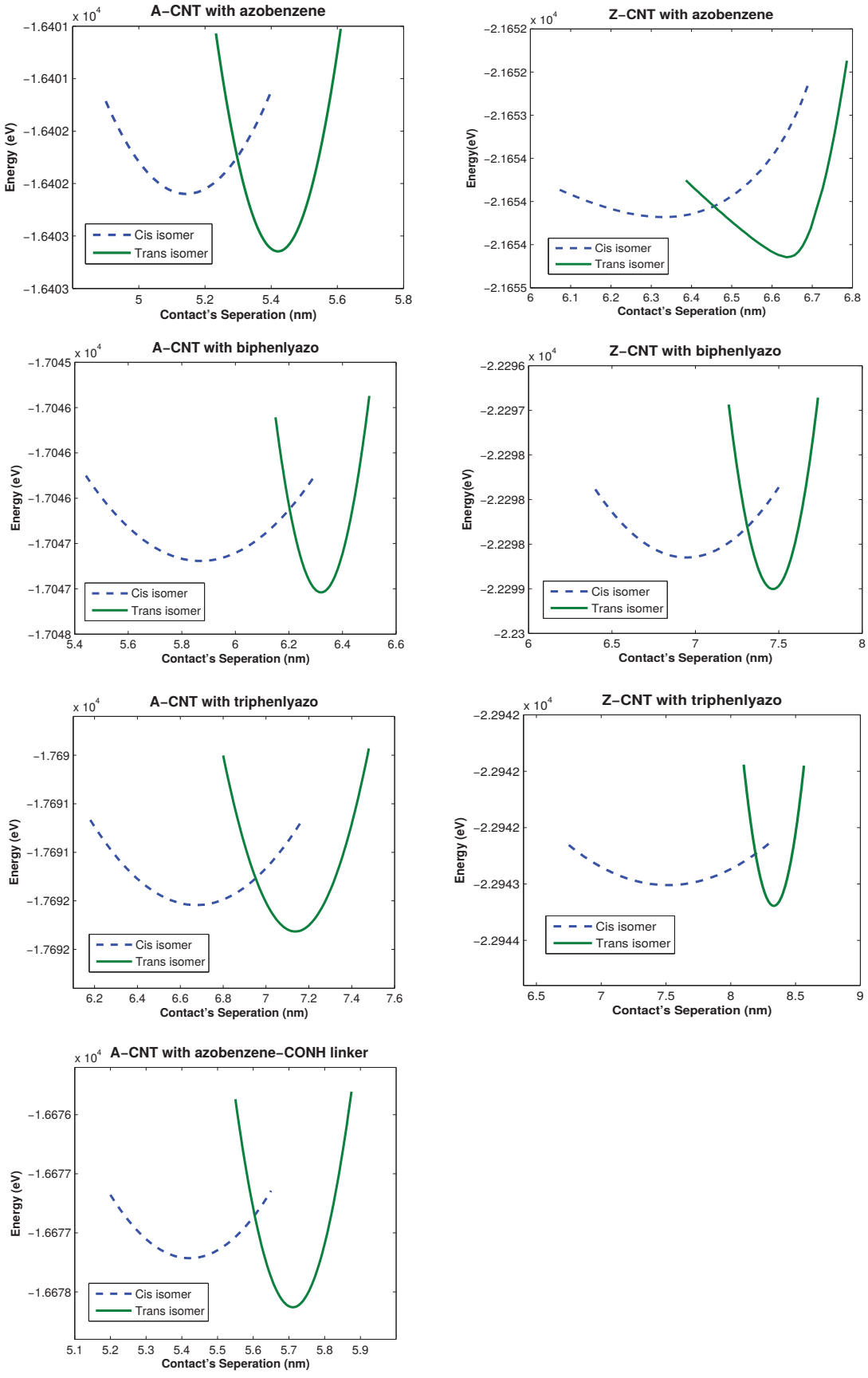

Figure 4.1. Energies vs Contacts Seperations

azobenzene molecule's lenght is shorter than the lenght of its derivatives, some tension remains on the linkers. While the lenght of molecules are getting longer, the energy differences dissappear. Furthermore, in the low energetic configurations the direction of the *cis* isomer bendings differs from each other according to the types of reservoirs and linkers. Each type of low energetic configuration will be deeply investigated in the upcoming sections.

4.2. Azobenzene

In this section, the investigation is on the system in which azobenzenes are used as junctions. Because azobenzene is the main molecule of this study, this section is completely dedicated to azobenzene. Transmissions of the systems are shown in figure 4.2. The left graph represents the case where reservoirs consist of armchair carbon nanotubes, and the right one illustrates the transmission of the system in which reservoirs consist of zigzag carbon nanotubes. The blue lines represent the *cis* isomeric state of azobenzene, while the green lines represent the *trans* isomeric state of azobenzene in both cases. At low frequencies, isomers' transmissions are similar to each other, however, within high frequency range, the difference between the transmission spectrum of the isomers becomes evident.

The conductivity plot can be seen in the figure 4.3. The green, blue, turquoise, and red lines represent armchair carbon nanotubes with *trans* isomer, armchair carbon nanotubes with *cis* isomer, zigzag carbon nanotubes with *trans* isomer, and zigzag carbon nanotube with *cis* isomer, respectively. The most conductive one of these systems is the system in which reservoirs are constructed from armchair carbon nanotubes, and where the junction is in *trans* isomeric state. *Trans* isomer is more conductive than *cis* isomer in both cases. If we compare carbon nanotube's isomers in itself, the system in which thermal reservoirs are made up from armchair carbon nanotubes is more conductive than the system where thermal reservoirs are made from zigzag carbon nanotubes. The switching effect of the system where armchair carbon nanotubes are used as reservoirs is 19.81% while the switching effect of the other is 20.58 %. For a better understanding, low energetic configurations are illustrated in the figure 4.4. The structures located at left side of the figure demonstrate the armchair reservoir case while the structures located at the right side of the figure represent the zigzag reservoir case. The upper illustrations belong to *cis* isomeric states, the below illustrations belong to *trans* isomeric states. If low energetic configurations are examined, one can see the reason for why switching effects are close to

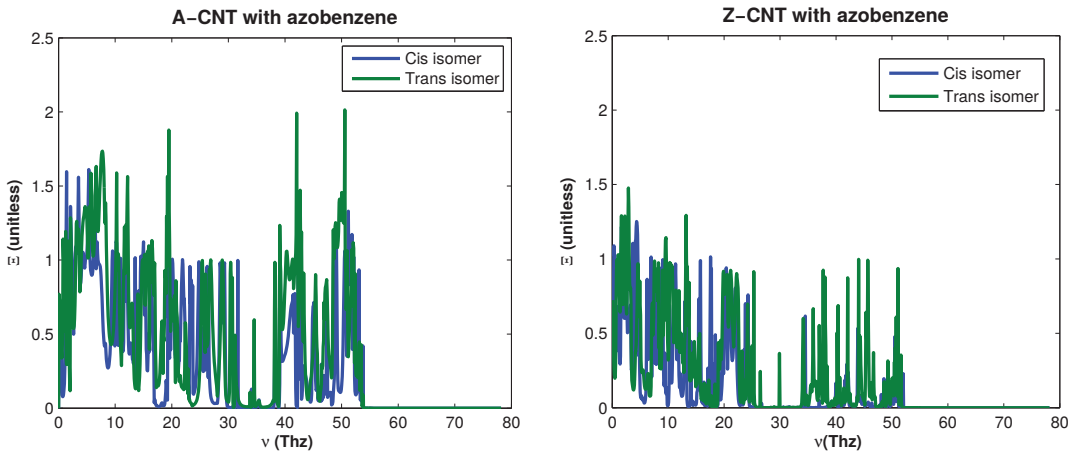

Figure 4.2. Transmission graphs of azobenzene with armchair carbon nanotube (left) and with zigzag carbon nanotube (right)

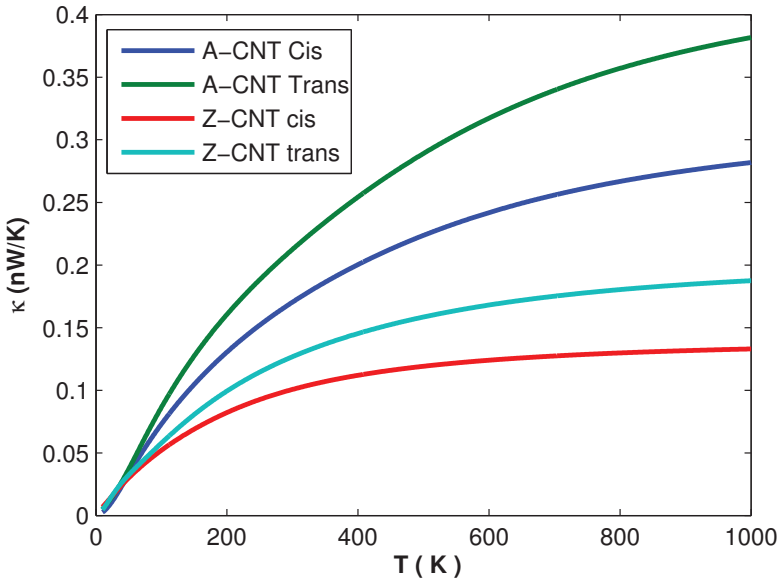

Figure 4.3. Conductances of armchair CNT with azobenzene's isomers and zigzag CNT with azobenzene's isomer

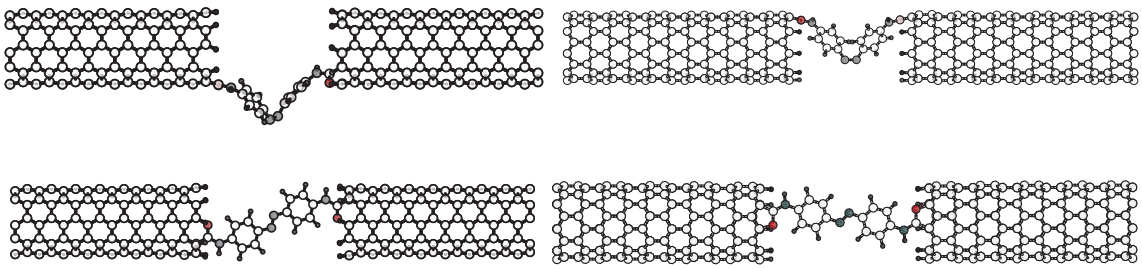

Figure 4.4. Low energy configurations of *cis* isomer of azobenzene contacted with armchair carbon nanotube (up-left), *trans* isomer of azobenzene contacted with armchair carbon nanotube (bottom-left), *cis* isomer of azobenzene contacted with zigzag carbon nanotube (up-right), *trans* isomer of azobenzene contacted with zigzag carbon nanotube (bottom-right)

each other while conductances are different. Although, *cis* isomers bend to the opposite directions in respect to one another, their bending is similar in both cases. This can be seen clearly in the upper illustrations of the figure 4.4. To support this condition, linker angles (measured from CNC one carbon belongs to reservoir, linker's nitrogen and the other carbon is located the para position of the benzene) are measured, see table 4.1. Angles' values are close to each other, which means that the stress upon the linkers is similar. As a result, the structural difference between two isomeric states is alike, and switching effect remains the same under change of reservoirs between zigzag carbon nanotube and armchair carbon nanotube.

Table 4.1. Angle of linkers connects azobenzene to reservoirs

Thermal reservoir	Left angle	Right angle
Armchair CNT	124.313	124.291
Zigzag CNT	124.720	125.159

4.3. Effect of Molecule

In this part, the use of different molecules as junctions and the effect of this usage is investigated. To be more precise, the junctions are constructed by using azobenzene derivatives, i.e. azobiphenly and azotriphenly. In the figure 4.5, the graph on the left side shows the transmission plot of the system where the junction is a single azobiphenly molecule and the reservoirs are constructed from armchair carbon nanotubes, and the graph on the right side represents the transmission plot of the system in which reservoirs are constructed from zigzag carbon nanotubes. The blue lines indicate the *cis* isomeric states, while the green lines indicate the *trans* isomeric states. In the figure 4.7, apart from junctions being constructed from azotriphenly molecules, all the attribute are the same as in figure 4.5. The difference in transmission spectrum of isomers descends as opposed to expectation.

Figures 4.6 and 4.8 demostrate the graphs of conductances. In the figure 4.6, the junctions of systems are established by using azobiphenly molecules, however, reservoirs are different in terms of carbon nanotube's isomers. The blue, green, red, and turquoise lines indicate armchair reservoir with *cis* isomeric junction, armchair reservoir with *trans* isomer, zigzag reservoir with *cis* isomer, and zigzag reservoir with *trans* isomer, respectively. This order is valid for the figure of conductance, in which azotriphenly is used as junction molecule. It can be clearly seen from the figures of conductance that when the systems are at *trans* isomeric states, the conductivity increases as opposed to the conductance in *cis* isomeric states, as in azobenzene case. In addition, the systems in which isomers are bound to zigzag carbon nanotubes are less conductive than the systems in which isomers are bound to armchair carbon nanotubes.

Table 4.2 demonstrates both switching effects and conductances at 300K. Switching effects of azobiphenly case shows different behaviour. When the junction is azobiphenly, and armchair carbon nanotubes are used as thermal reservoirs, switching effect is 17.90% while switching effect of zigzag carbon nanotube's case is 9.53% as opposed to the trend azobenzene and azotriphenly have established. When reservoirs are changed from armchair carbon nanotubes to zigzag carbon nanotubes, their switching effects remain approximately the same. The reason of this difference can be clearly understood from low energetic configurations. Figure 4.9 demonstrates the bridges of systems, their junctions are constructed by using azobiphenly molecules. When *trans* isomer is bound to zigzag carbon nanotube, its planarity disappears. However, in armchair case, planarity of *trans* isomer is unspoiled.

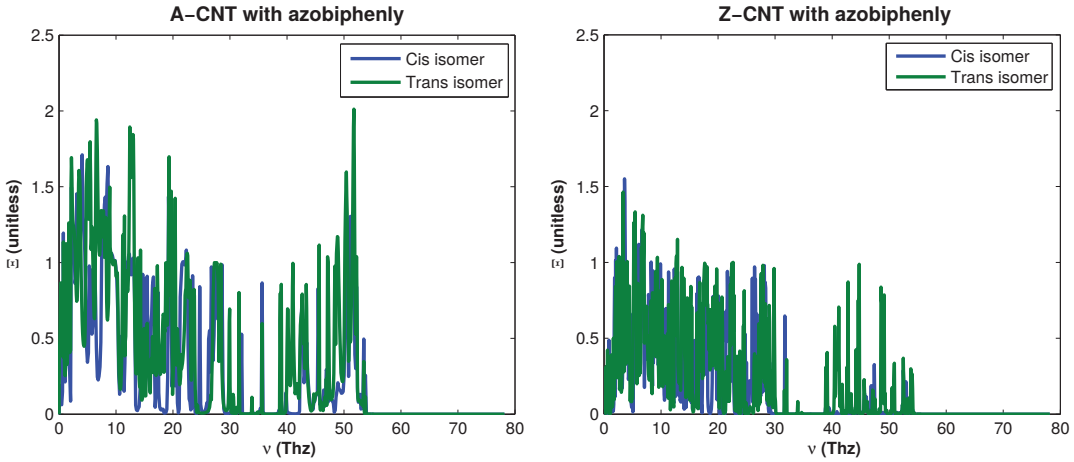

Figure 4.5. Plot of transmissions of armchair CNT with azobiphenly's isomers is on the left. Plot of transmissions of zigzag CNT with azobiphely's isomers is on the right.

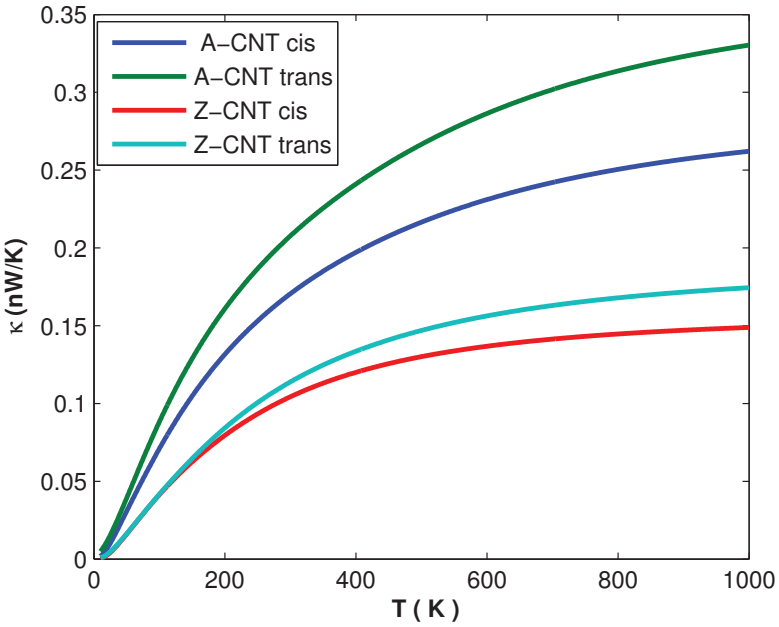

Figure 4.6. Plot of conductances of azobiphenly with both isomer of CNTs

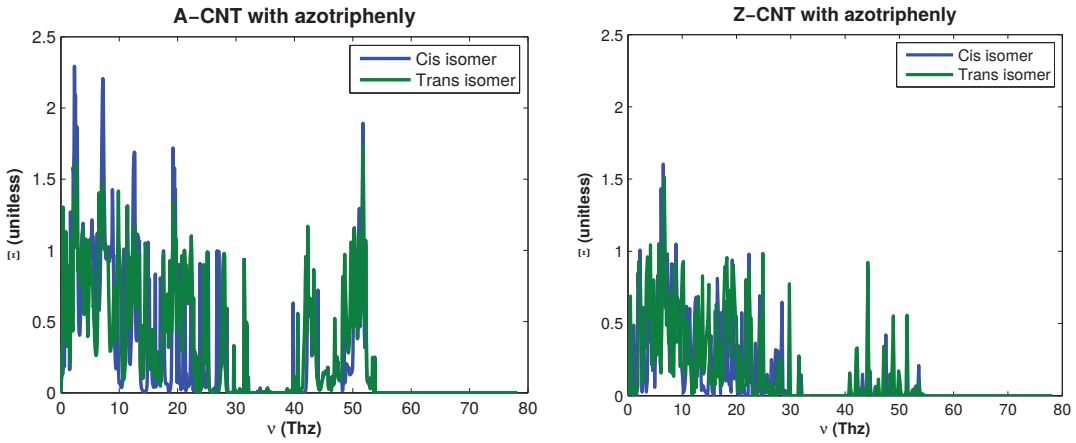

Figure 4.7. Plot of transmissions of armchair CNT with azotriphenly's isomers is on the left. Plot of transmissions of zigzag CNT with azotriphely's isomers is on the right.

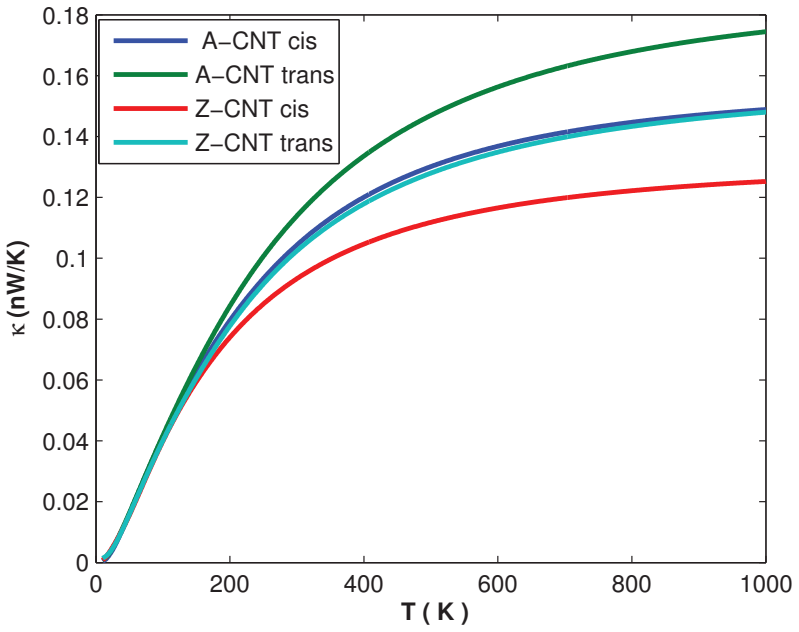

Figure 4.8. Conductances of isomers of *cis* azotriphenly linked to armchair carbon nanotubes(blue line), linked to zigzag carbon nanotube(red line), conductances of *trans* isomer linked to armchair carbon nanotubes(green line), linked to zigzag carbon nanotube (turqouse line)

Table 4.2. Switching effects of systems

Thermal reservoir	Junction Molecule	*cis* Isomer (nW/K)	*trans* Isomer (nW/K)	Switching Effect
A- CNT	Azobenzene	0.1704	0.2125	19.81%
	Azobiphenly	0.1706	0.2078	17.90%
	Azotriphenly	0.1044	0.1144	8.74 %
Z-CNT	Azobenzene	0.1007	0.1268	20.58%
	Azobiphenly	0.1044	0.1154	9.53%
	Azotriphenly	0.933	0.1024	8.11 %

Table 4.3. Dihedral angles of *cis* isomers

Molecule	Free Molecule	Linked to A-CNT	Linked to Z-CNT
Azobenzene	13.943 deg	26.268 deg	18.413 deg
Azobiphenly	13.419 deg	18.559 deg	15.167 deg
Azotriphenly	13.496 deg	17.881 deg	13.546 deg

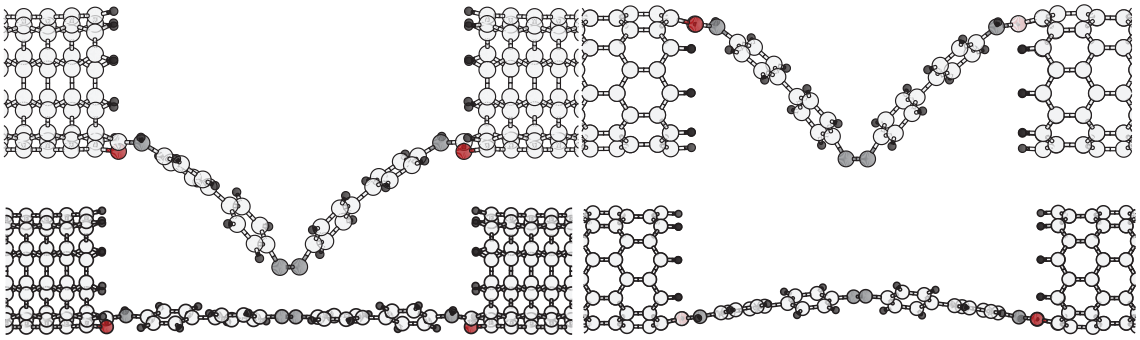

Figure 4.9. Bridge structures of *cis* azobiphenly with armchair CNT (top left), *trans* azobiphenly with armchair CNT (bottom left), *cis* azobiphenly with zigzag CNT (top right), and *trans* azobiphenly with zigzag CNT (bottom right)

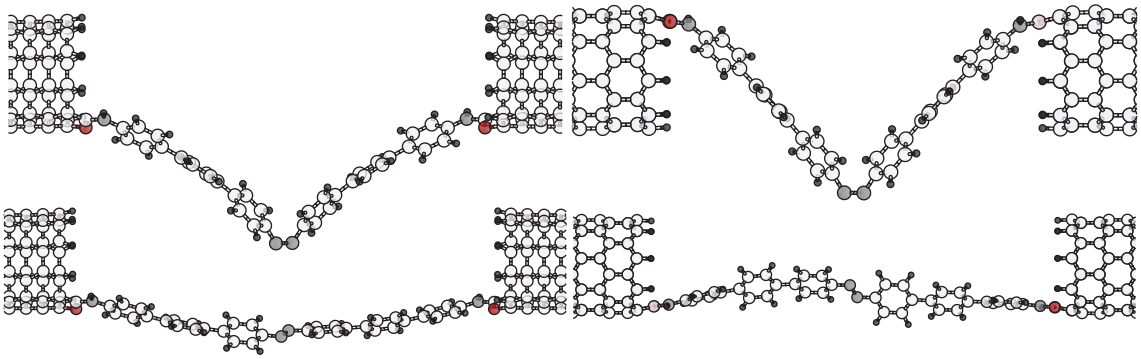

Figure 4.10. Bridge structures of *cis* azotriphenly with armchair CNT (top left), *trans* azotriphenly with armchair CNT (bottom left), *cis* azotriphenly with zigzag CNT (top right), and *trans* azotriphenly with zigzag CNT (bottom right)

When the low energetic structures of junctions with azotriphenly are examined, the observed case become stranger. The benzene rings of triphenly rotate, and as a result, the perfect geometry of free azotriphenly's isomers break down. The motivation to use longer molecules as junctions was to improve the switching effect via enhanced folding. Since the azobenzene is a short molecule, linked *cis* isomer's folding can not be achieved completely, and as a result, some stress remains on linkers and switching effect is low as opposed to expectations. Table 4.3 shows dihedral angles between *cis* isomer's planes. The most significant change happens in azobenzene case; while the dihedral angle of *cis* azotripenly, which is linked to the zigzag carbon nanotube, remains almost the same as free molecule. Extended molecules are expected to remove these deviations from the free molecule's behaviour. However, two other effects disprove this expectation. The first one is that when the molecules are extended, their spectrum becomes denser, which means that the number of channels where phonons flow through will increase. This effect improves the conductance while it reduces the switching effect. The second effect is that the structures of azobiphenly and triphenly molecules are degenerated when connections are set. The benzene rings are flipped. The most significant degenerations occur in azotriphenly cases. See figure 4.10. *Trans* azotriphenly loses its planarity in each case. As a result, conductances are low, as well as switching effects.

4.4. Effect of Reservoir

In this section, the effects of using different linkers are analysed. To see the effects in the usage of different reservoirs, two different kinds of carbon nanotubes are used: armchair carbon nanotube and zigzag carbon nanotube. Besides, generic reservoirs are derived by using sound velocity, as explained previously in the Methods chapter. Because the molecules are degenerated due to the connections, the state of the generic reservoir clearly displays the switching effect where this degeneration is kept out. In other words, it lays bare the difference between the *cis* and *trans* isomer states. Furthermore, before a system is established, one can predict the transport characteristics of a molecule which is intended to be used as the junction, by virtue of the fact that it favours and accelerates the calculation process. Figure 4.11 demonstrates the transmissions of constructions, in which junctions are build by use of azobenzene molecules. At left graphic displays transmissions of junctions with *cis* isomer of azobenzene molecule, and the one located at right side of the figure 4.11 displays transmissions of juctions with *trans* isomers. In both cases, red lines, green lines, and blue lines point toward zigzag carbon nanotube

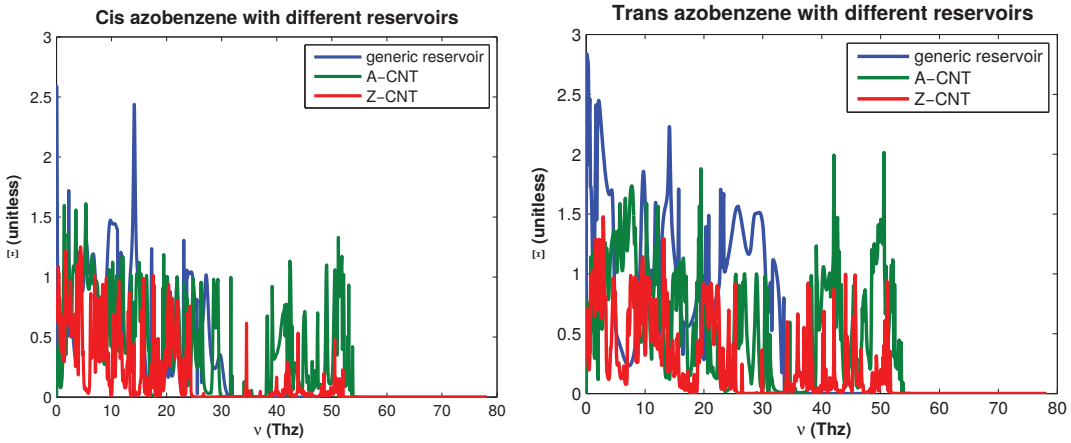

Figure 4.11. Transmissions of azobenzene isomers linked to different reservoirs. Graphic at left side demonstrates transmissions of *cis* isomers linked to different reservoirs, at right side transmisions of *trans* isomers linked to different reservoirsare seen. Red lines indicate zigzag carbon nanotubes, green lines indicate armchair carbon nanotube, and blue lines indicate generic reservoirs

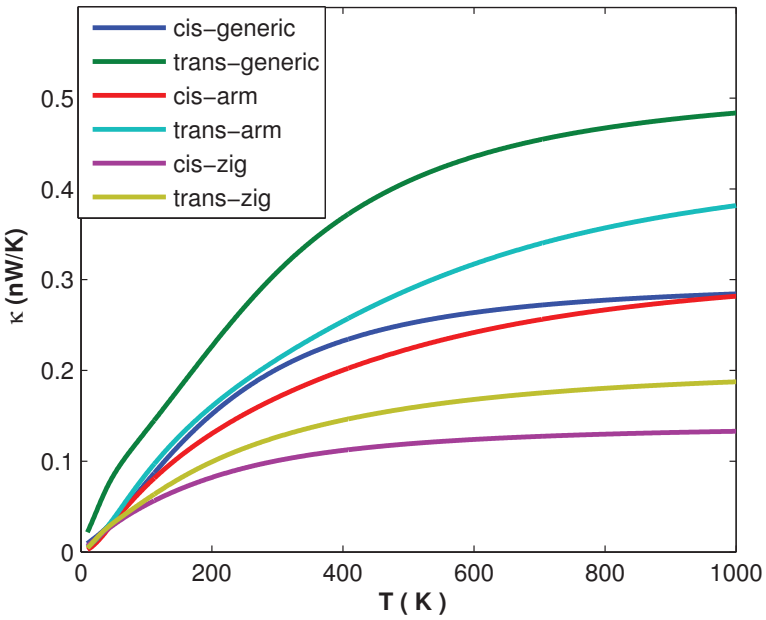

Figure 4.12. Conductances of azobenzene isomers with different reservoirs

reservoirs, armchair carbon nanotube reservoirs, generic reservoirs, respectively. Due to the fact that sound velocity describes acoustic phonons, frequency range become narrow, and maximum frequency drops in case of generic reservoirs.

Figure 4.12 demonstrates the conductances of the construction with azobenzene junctions linked to different thermal reservoirs. The *cis* isomer, which is linked to zigzag carbon nanotube, armchair carbon nanotube, and generic reservoir point toward purple, red, and blue line, respectively; and for *trans* isomer; yellow, turquois, green lines indicate the reservoirs in the same order. Table 4.4 shows the numerical results that are obtained at 300 K. The most conductive system includes *trans* isomer of azobenzene as junction and its reservoirs are described by generic reservoirs. The generic reservoirs yield elevated conductances, because of the stress effects as explained in the azobenzene section and deterioration effects as explained in the effect of molecule section are removed. In systems where zigzag carbon nanotubes are used as thermal reservoirs, the conductances are low. The conductances of bare carbon nanotubes in armchair and zigzag form at 300 K is 2.8774 nW/K and 2.7944 nW/K, respectively. In despite of this resemblance, the conductance of the systems where zigzag carbon nanotubes are used as reservoirs are lower than the cases of armchair reservoirs. This condition is related with the distribution of the modes on the device. The distribution of the modes is going to be investigated thoroughly in the last section of this chapter. The justification of why switching effects remain the same, despite the fact that conductance deviates significantly from each other under the changeover of reservoirs between armchair carbon nanotube and zigzag carbon nanotube, was clearly stated in azobenzene section.

Table 4.4. Switching effects of systems in which azobenzene linked to different reservoirs

Reservoir	*cis* isomer	*trans* isomer	Switching effect
Armchair CNT	0.1704 nW/K	0.2125 nW/K	20.01 %
Zigzag CNT	0.1007 nW/K	0.1268 nW/K	20.58%
Generic Reservoir	0.1993 nW/K	0.3056 nW/K	34.62 %

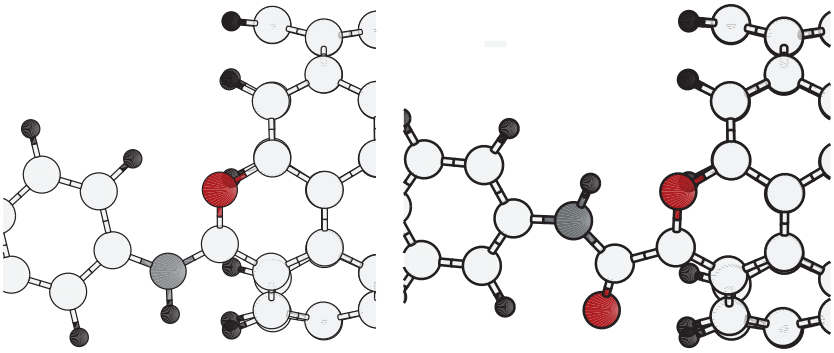

Figure 4.13. This is a close look of the connections between the contacts and the azobenzene molecule. The geometry of the NH linker is illustrated at left, while geometry of $CONH$ linker is illustrated at right.

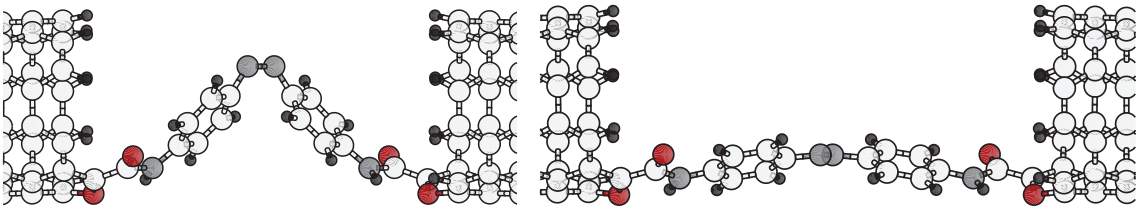

Figure 4.14. Bridge structures of *cis* azobiphenly linked to armchair CNT by $CONH$ linker (left), *trans* azobiphenly linked armchair CNT by $CONH$ linker (right)

4.5. Effect of Linker

In this section, the effects of changeover linkers from NH to $CONH$ linker are investigated. Up to this point, NH linker establishes connections between contacts and molecules to reservoirs in each case. Additional CO atoms are placed between the contacts and the NH linker to form $CONH$ linker, see figure 4.13. For a clear statement, azobenzene molecule is connected to armchair carbon nanotube reservoirs and generic reservoirs by both NH and $CONH$ linkers. To illustrate the junctions clearly, figure 4.14 demonstrates low energetic bridge structures of the case where azobenzene molecule is linked to armchair carbon nanotubes by $CONH$ linker. If we compare figure 4.4 and figure 4.14, some structural differences are observed. The direction of the *cis* isomer bending is reversed as opposed to the case where azobenzene molecule is bound by NH linker to armchair carbon nanotubes. Besides, *trans* isomer planarity is not perfect, a

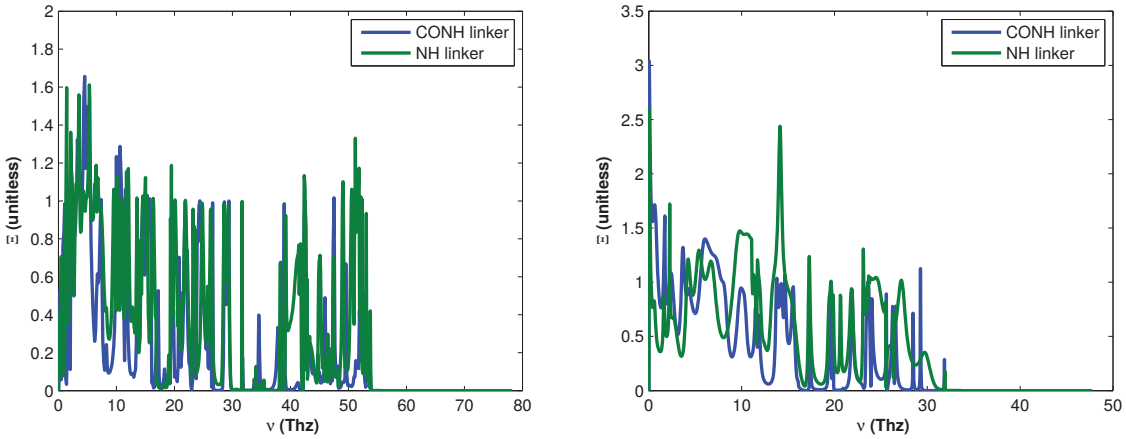

Figure 4.15. Transmissions of *cis* isomers of azobenzene which is bound by both $CONH$ linker (blues lines) and NH linker (green lines) to armchair carbon nanotube reservoir (left) and generic reservoir (right)

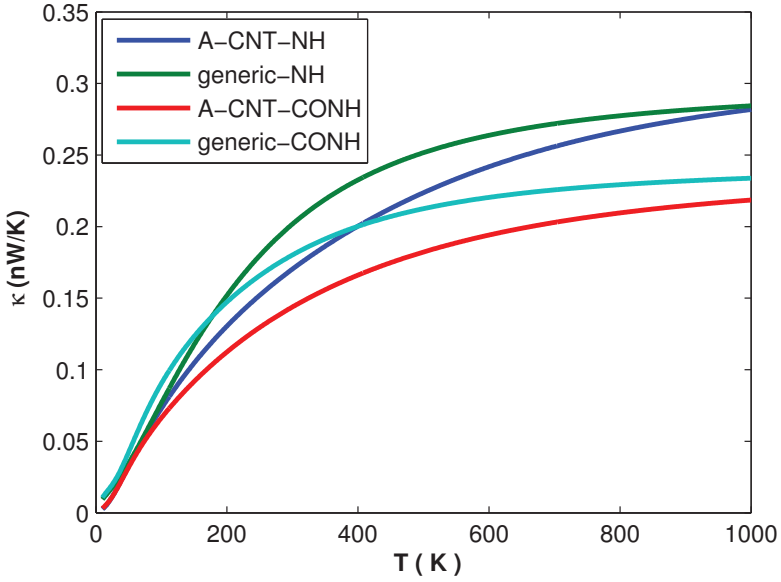

Figure 4.16. Conductances of *cis* isomers which is connected to both armchair and generic reservoirs by two different linker group

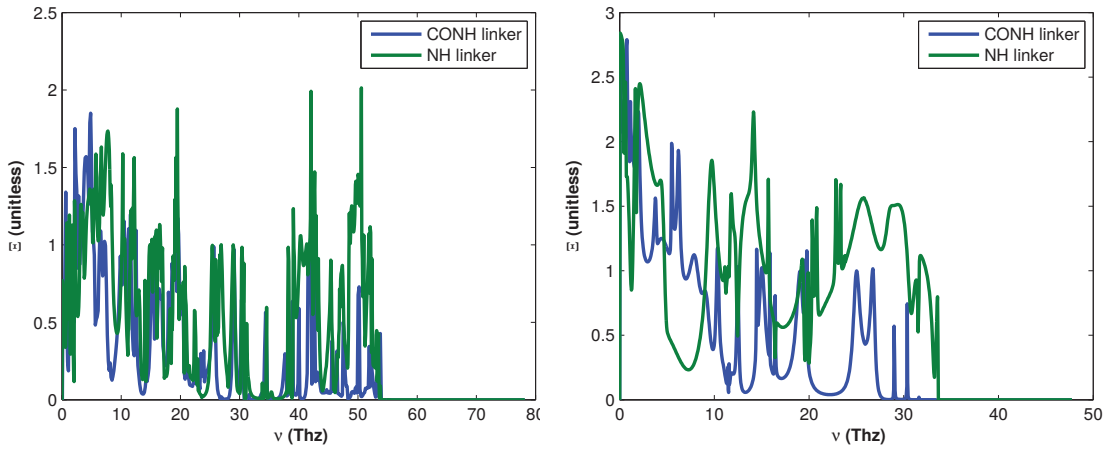

Figure 4.17. Transmissions of *trans* isomers of azobenzene which is bound by both $CONH$ linker (blues lines) and NH linker (green lines) to armchair carbon nanotube reservoir (left) and generic reservoir (right)

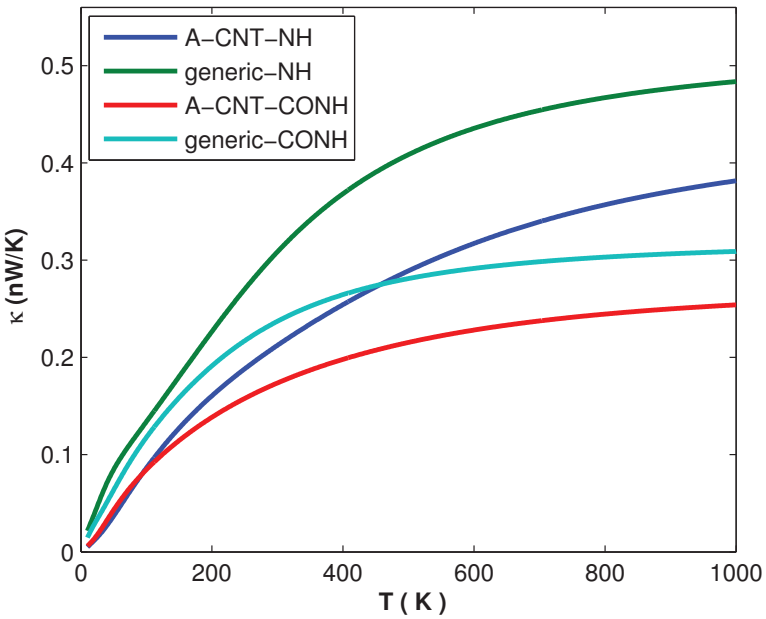

Figure 4.18. Conductances of *trans* isomers which is connected to both armchair and generic reservoirs by two different linker group

slight bending in the *trans* isomer is observed and its benzen rings have rotated a little. Figures 4.15 and 4.17 demonstrate the transmission graphics. Isomers are separated to get an explicit illustration. In all four transmission graphs, blues lines represent $CONH$ linker case, green lines represent NH linker case. Using $CONH$ rather than NH as the linker lowers the transmission in all cases. This decrease can be observed much better in the transmission graphs with generic reservoirs. As it is understood from all the transmission graphs, the difference is significant at high frequencies.

Figures 4.16 and 4.18 show conductances. Figure 4.16 stands for *cis* isomer in four different cases: connected to armchair carbon nanotube by NH linker (blue line), connected to generic reservoir by NH linker (green line), connected to armchair carbon nanotube by $CONH$ linker (red line), connected to generic reservoir by $CONH$ linker (turquois line). Figure 4.18 illustrates conductances of trans isomers in the same manner. In each cases, usage of $CONH$ connector group instead of NH connector group lowers the conductances as well as switching effects. When using $CONH$ linker, the switching effect where azobenzene is connected to armchair reservoirs and generic reservoirs is 17% and 22%, respectively. The distortion in *trans* isomer, as mentioned in the beginning of this section, lowers the switching effect in armchair reservoir case. The reason why conductances and switching effects are low in the case of $CONH$ linker is going to be investigated more deeply in the Mode Analysis section.

4.6. Mode Analysis

Up to now, we discussed the transmissions and the conductances by relating them to the low energetic configurations. In this section, the atomic displacements are visualized to have deeper understanding. To achieve this, the self-energies are incorporated into the dynamic matrix, and eigenvectors and eigenvalues of the result matrix are calculated.

$$M = (\hat{D}_D + \Sigma_l + \Sigma_R) \tag{4.1}$$

$$Mu = \omega^2 u \tag{4.2}$$

where u represents displacements of the atoms at the frequency w. This calculation is done for frequencies that have significant differences. The animation videos of these frequencies are attached to this thesis additionally.

In the first two illustrations the connection case of our main molecule azobenzene

linked to the armchair carbon nanotubes by NH linker is investigated. In the first illustration of these two, the frequency of 23.4603 THz where the *cis* isomer transmission has higher value than the *trans* isomer transmission, and as to the second visual, the frequency of 42.0596 THz, where *trans* isomer transmission has higher value than than the *cis* isomer is examined. The turquoise arrows show displacements. What draws the attention in these displacements are that while the modes in the *cis* isomer are uniform and distributed properly, the displacements in the *trans* isomer molecule are lacking. However, in the second illustration the contrary is observe: while the modes in the *trans* isomer are distributed properly, the displacements in the *cis* isomer molecule atoms are poor.

Looking the following two illustrations the focus is on why the $CONH$ linker usage linkers lowers the conductances. In the first of these illustrations the *cis* isomeric state is visualized and in the second one, *trans* isomeric state is visualised. As one observes in both cases, it is clear that the displacements of molecules atoms are poor in the case usage of $CONH$ linker. Modes are aggregated on the reservoirs. Especially when when we look at the visual where *cis* isomer state has been drawn what stands out is the arrows that belong to the oxygen atoms which complete the hexagons of the armchair carbon nanotubes. This reveals that additional CO atoms behave like a barrier to the coming phonons.

In the last figure, the focus of interest is that why there is a difference between conductances of the armchair reservoir case and zigzag reservoir case, even though there is almost no difference between the conductivities of bare armchair carbon nanotubes and zigzag carbon nanotubes. In the figure 4.23, the left illustrations stands for *cis* isomer and the *trans* isomer is illustrated at right. Modes are distributed on the system asymmetrically. Displacements of atoms which belong to the system with *cis* isomeric junction are determined at 38 THz while displacements of atoms which are belong to the system with *trans* isomeric junction are determined at 33 THz. At these frequencies, transmission values of both systems are close to zero. Visualisation of the displacements reveals that vibrational modes have an asymmetric distribution. This is the reason why the systems with zigzag reservoirs have lower conductances than the systems with armchair reservoirs.

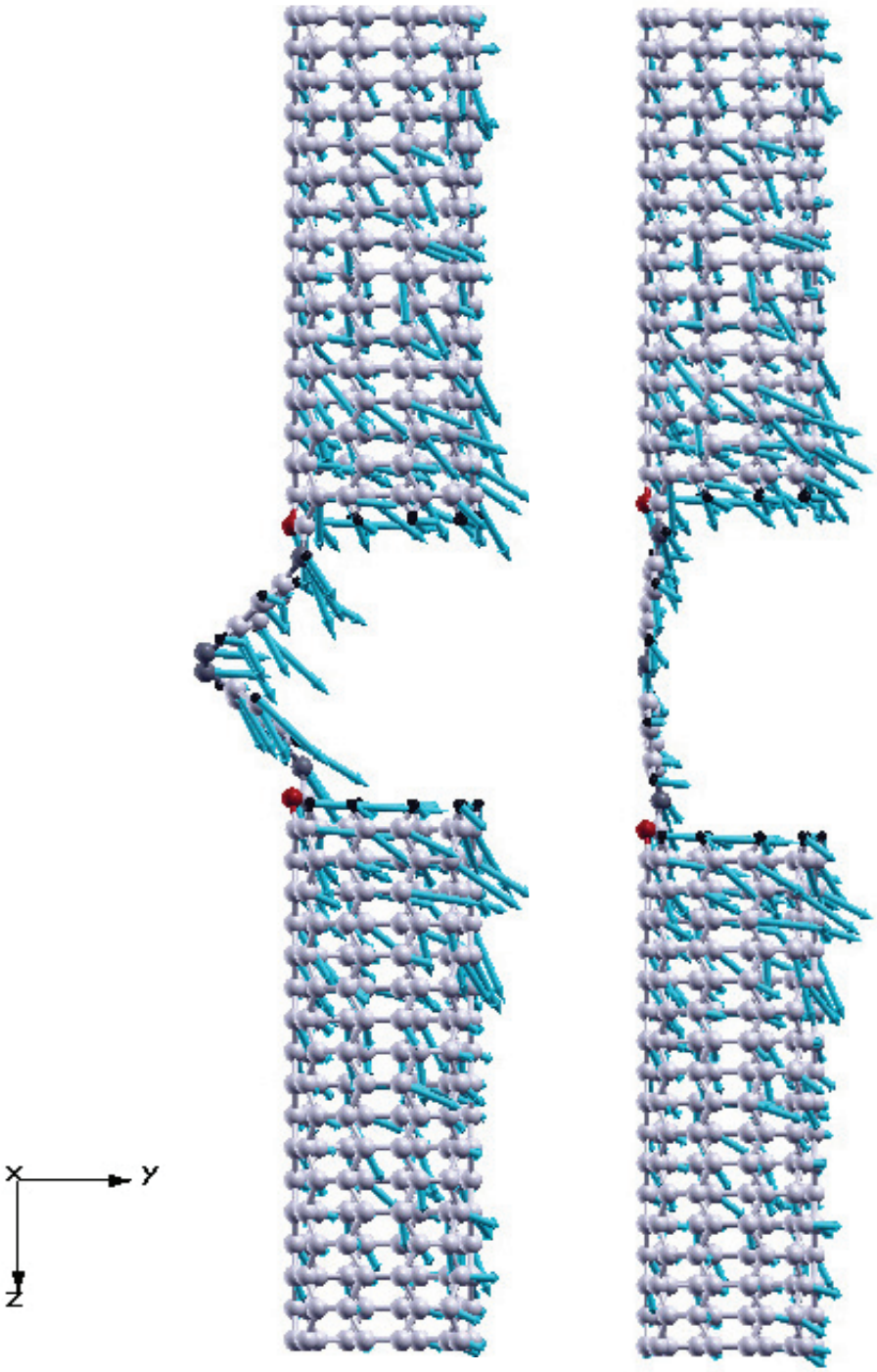

Figure 4.19. Visualization of atoms' displacements. The systems contain armchair carbon nanotubes, azobenzene molecule, and NH linkers. The displacements are calculated at the frequency, 23.4603 THz. The left illustration shows the *cis* isomeric state and the one at right side demonstrates the *trans* isomeric state. At this frequency, the *cis* isomeric state has a higher transmission value than the *trans* isomeric state.

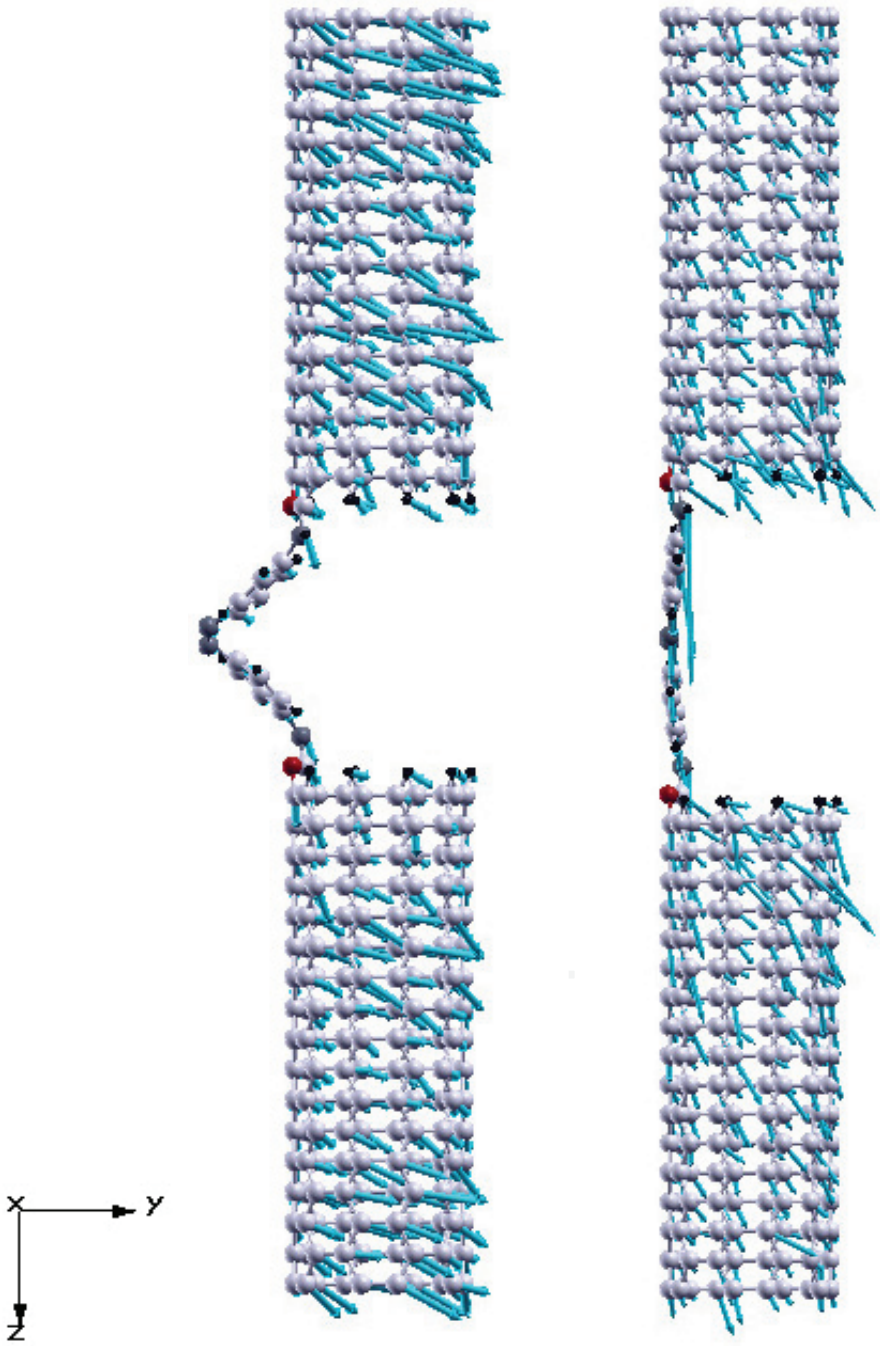

Figure 4.20. In this illustration the same system of the figure 4.19 is shown. But here, the displacements are determined at 42.0596 THz. At this frequency, the *trans* isomeric state has a higher transmission value than the *cis* isomeric state. This can be observed by looking at the arrows that belong to the linkers.

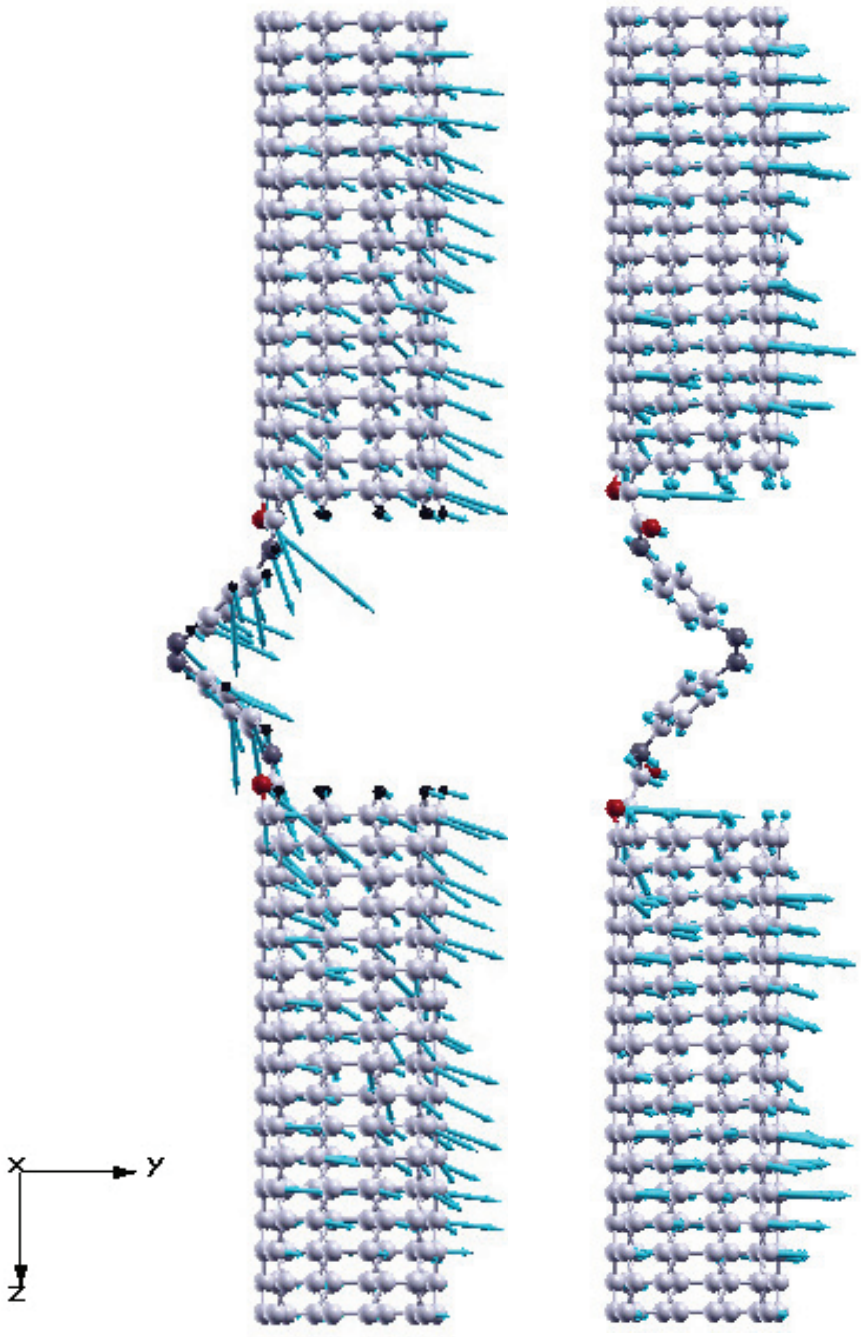

Figure 4.21. The linkers are compared with each other by the visualisation of the systems where azobenzene molecule is linked to armchair carbon nanotubes by the NH linker(left) and the $CONH$ linker(right). Both systems are in the *cis* isomeric state. The frequency, 6.2533 THz, is selected to determine displacements. At this frequency, the polarization directions of the arrows, which belong to the linkers draw attantion. The $CONH$ linker behaves like a barrier.

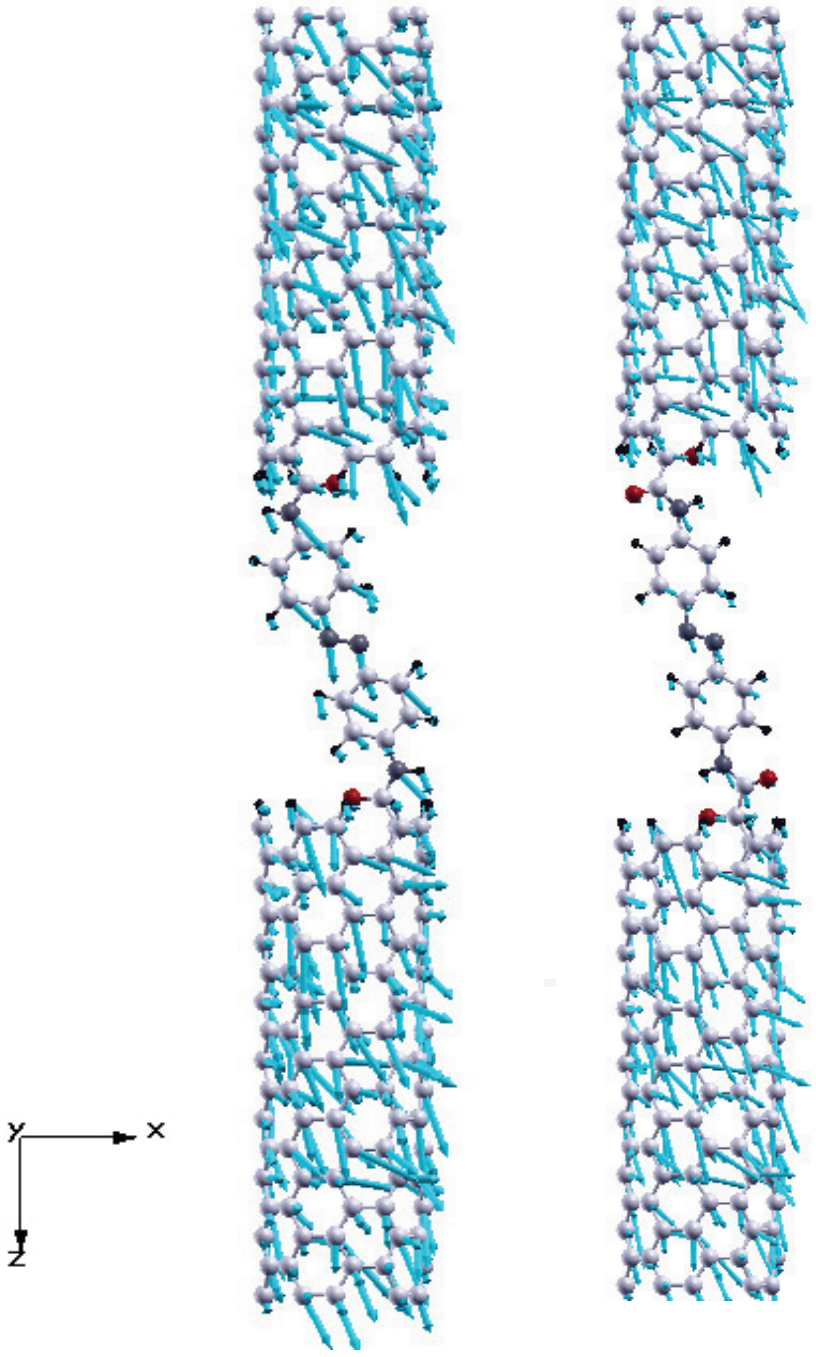

Figure 4.22. In this figure, the same systems in the same order as the figure 4.21 is discussed to compare linkers. But these systems are in *trans* isomeric state. The displacements have been calculated at the frequency, 27.3851 THz. And the results show that the vibration of the molecule with the $CONH$ linker is poor.

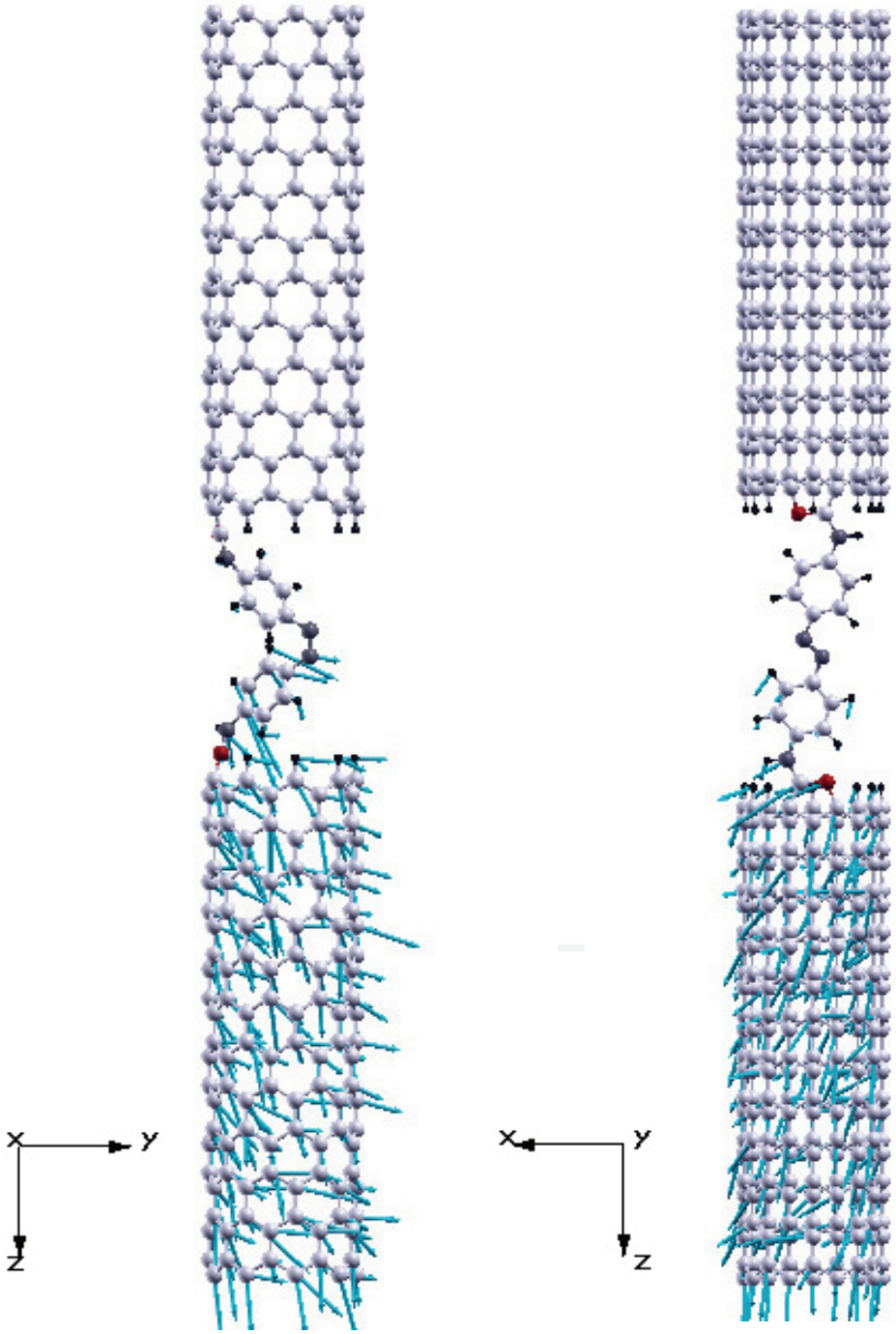

Figure 4.23. This illustration shows the system where zigzag carbon nanotubes are linked to the azobenzene molecule by NH linker. The junction that is illustrated at left is in the *cis* isomeric state while the juction that is illustrated at right is in the *trans* isomeric state. The displacements that are seen at the left visual are calculated at 38 THz frequency, while displacements of the right one are calculated at 33 THz. The transmission values at both frequencies are approximately zero, because there is an asymmetric distribution of vibrational modes.

CHAPTER 5

CONCLUSION

To sum up, in this thesis; the possibility of the heat flow control based on both photoisomeric behaviour of azobenzene and its derivatives, and single molecule junction is investigated to build a thermal switch. A singular molecule junction is a structure where a single molecule is placed between two semi-infinite reservoirs. In this thesis, to build the switch, a single azobenzene molecule or one of its derivatives is placed between two semi-infinite carbon nanotubes. These photoisomeric molecules change their three-dimensional structures when exposed to light in particular frequencies. The possibility whether the thermal flux can be altered between on and off states by the help of the photo isomeric behaviour of the molecules is examined. The effects of linker groups, thermal reservoirs, and different molecules on thermal conductivity are analysed as well. The findings indicate that the structural changes of the molecules can alter the thermal conductivity with a fair average. *Trans* isomers of molecules are found to be more conductive than *cis* isomers. Azobenzene derivatives are used as well, because with the extension of the molecules it was expected that the switching effect would increase. As the molecules are extended, the stress on the linkers that connect the azobenzene with the carbon nanotubes decreases. Because of that, the prediction was an increase of the switching effect that originated from this decrease of stress. However, a decrease was observed on the switching effect for the reason that there where distortions when molecules are extended. In addition, two different kinds of chiral isomers of carbon nanotube - armchair and zigzag - are used as thermal reservoirs, moreover on the account of a deeper understanding of these systems' behaviour, generic reservoirs are developed. The results of developing generic reservoirs reveal that the deterioration of the azobenzene molecule, which occurs when the connections are established, reduces the intended switching effect. The changeover of reservoirs brings out the obvious that the switching effect does not directly depend on the chirality of carbon nanotubes that are used as thermal reservoirs. Changeover of the reservoirs from armchair carbon nanotube to zigzag nanotube alter the conductances, but without changing the switching effect. Extension of the linker by adding CO-group into to NH-group lowers the thermal conductivity, besides switching effect, due to the fact that additional atoms are able to act like barriers.

REFERENCES

[1] Longji Cui, Wonho Jeong, Sunghoon Hur, Manuel Matt, Jan C. Klöckner, Fabian Pauly, Peter Nielaba, Juan Carlos Cuevas, Edgar Meyhofer, and Pramod Reddy. Quantized thermal transport in single-atom junctions. *Science*, 355(6330):1192–1195, 2017.

[2] A. Beiser. *Concepts of Modern Physics*. Physics series. McGraw-Hill, 1987.

[3] P. Atkins and J. de Paula. *Atkins' Physical Chemistry*. OUP Oxford, 2010.

[4] Albert Einstein. Die plancksche theorie der strahlung und die theorie der spezifischen wärme. *Annalen der Physik*, 327(1):180–190, 1906.

[5] S.H. Simon. *The Oxford Solid State Basics*. OUP Oxford, 2013.

[6] P. Debye. Zur theorie der spezifischen wärmen. *Annalen der Physik*, 344(14):789–839, 1912.

[7] G.P. Srivastava. *The Physics of Phonons*. Taylor & Francis, 1990.

[8] P. Hofmann. *Solid State Physics An Introduction*. Physics textbook. Wiley, 2011.

[9] C. Kittel. *Introduction to Solid State Physics*. Wiley, 2004.

[10] Lei Wang and Baowen Li. Phononics gets hot. *Physics World*, 21(03):27, 2008.

[11] Martin Maldovan. Sound and heat revolutions in phononics. *Nature*, 503(7475):209–217, Nov 2013. Review.

[12] Nianbei Li, Jie Ren, Lei Wang, Gang Zhang, Peter Hänggi, and Baowen Li. Colloquium. *Rev. Mod. Phys.*, 84:1045–1066, Jul 2012.

[13] Chih Wu. Analysis of waste-heat thermoelectric power generators. *Applied Thermal Engineering*, 16(1):63 – 69, 1996.

[14] Rachel Berkowitz. Energy focus automotive industry drives search for tunable thermal switch materials. *MRS Bulletin*, 42(1):7 7, 2017.

[15] E. Pallecchi, Z. Chen, G. E. Fernandes, Y. Wan, J. H. Kim, and J. Xu. A thermal diode and novel implementation in a phase change material. *Mater. Horiz.*, 2:125–129, 2015.

[16] M. Dietrich, A. Euler, and G. Thummes. A lightweight thermal heat switch for redundant cryocooling on satellites. *Cryogenics*, 83:31 – 34, 2017.

[17] Alexander A. Balandin and Denis L. Nika. Phononics in low-dimensional materials. *Materials Today*, 15(6):266 – 275, 2012.

[18] Liang Guo, Xusheng Zhang, Yong Huang, Richa Hu, and Chunlong Liu. Thermal characterization of a new differential thermal expansion heat switch for space optical remote sensor. *Applied Thermal Engineering*, 113:1242 – 1249, 2017.

[19] Riccardo Bosisio, Stefano Valentini, Francesco Mazza, Giuliano Benenti, Rosario Fazio, Vittorio Giovannetti, and Fabio Taddei. Magnetic thermal switch for heat management at the nanoscale. *Phys. Rev. B*, 91:205420, May 2015.

[20] Wei-Rong Zhong, Dong-Qin Zheng, and Bambi Hu. Thermal control in graphene nanoribbons: thermal valve, thermal switch and thermal amplifier. *Nanoscale*, 4:5217–5220, 2012.

[21] Qian Li, Ivan Duchemin, Shiyun Xiong, Gemma C. Solomon, and Davide Donadio. Mechanical tuning of thermal transport in a molecular junction. *The Journal of Physical Chemistry C*, 119(43):24636–24642, 2015.

[22] M. Born and R. Oppenheimer. Zur quantentheorie der molekeln. *Annalen der Physik*, 389(20):457–484, 1927.

[23] R.M. Martin. *Electronic Structure: Basic Theory and Practical Methods*. Cambridge University Press, 2004.

[24] P. Hohenberg and W. Kohn. Inhomogeneous electron gas. *Phys. Rev.*, 136:B864–B871, Nov 1964.

[25] W. Kohn and L. J. Sham. Self-consistent equations including exchange and correlation effects. *Phys. Rev.*, 140:A1133–A1138, Nov 1965.

[26] D.J. Griffiths. *Introduction to Quantum Mechanics*. Pearson international edition. Pearson Prentice Hall, 2005.

[27] H. Chermette. Chemical reactivity indexes in density functional theory. *Journal of Computational Chemistry*, 20(1):129–154, 1999.

[28] Frank De Proft and Paul Geerlings. Conceptual and computational dft in the study of aromaticity. *Chemical Reviews*, 101(5):1451–1464, 2001. PMID: 11710228.

[29] Gotthard Seifert and Jan Ole Joswig. Density functional tight binding an approximate density functional theory method. *Wiley Interdisciplinary Reviews Computational Molecular Science*, 2(3):456–465, 2012.

[30] J. C. Slater and G. F. Koster. Simplified lcao method for the periodic potential problem. *Phys. Rev.*, 94:1498–1524, Jun 1954.

[31] R. P. Feynman. Forces in molecules. *Phys. Rev.*, 56:340–343, Aug 1939.

[32] Laurent Chaput, Atsushi Togo, Isao Tanaka, and Gilles Hug. Phonon-phonon interactions in transition metals. *Phys. Rev. B*, 84:094302, Sep 2011.

[33] A Togo and I Tanaka. First principles phonon calculations in materials science. *Scr. Mater.*, 108:1–5, Nov 2015.

[34] W. Zhang, T. S. Fisher, and N. Mingo. The atomistic green's function method: An efficient simulation approach for nanoscale phonon transport. *Numerical Heat Transfer, Part B: Fundamentals*, 51(4):333–349, 2007.

[35] Takahiro Yamamoto and Kazuyuki Watanabe. Nonequilibrium green's function approach to phonon transport in defective carbon nanotubes. *Phys. Rev. Lett.*, 96:255503, Jun 2006.

[36] A. Ozpineci and S. Ciraci. Quantum effects of thermal conductance through atomic chains. *Phys. Rev. B*, 63:125415, Mar 2001.

[37] W. Müller, R. Schiller, and W. Nolting. Understanding of surface states in a correlated electron system. *The European Physical Journal B - Condensed Matter and Complex Systems*, 16(4):705–718, 2000.

[38] I. M. De Rosa, F. Sarasini, M. S. Sarto, and A. Tamburrano. Emc impact of advanced carbon fiber/carbon nanotube reinforced composites for next-generation aerospace applications. *IEEE Transactions on Electromagnetic Compatibility*, 50(3):556–563, Aug 2008.

[39] Veena Choudhary and Anju Gupta. Polymer/carbon nanotube nanocomposites. In Siva Yellampalli, editor, *Carbon Nanotubes - Polymer Nanocomposites*, chapter 04. InTech, Rijeka, 2011.

[40] Miriam del Valle, Rafael Gutierrez, Carlos Tejedor, and Gianaurelio Cuniberti. Tuning the conductance of a molecular switch. *Nat Nano*, 2(3):176–179, Mar 2007.

[41] Silvio Osella, Paolo Samori, and Jerome Cornil. Photoswitching azobenzene derivatives in single molecule junctions: A theoretical insight into the i/v characteristics. *The Journal of Physical Chemistry C*, 118(32):18721–18729, 2014.

[42] Yan Wang and Hai-Ping Cheng. Electronic and transport properties of azobenzene monolayer junctions as molecular switches. *Phys. Rev. B*, 86:035444, Jul 2012.

[43] Emanuela Margapoti, Juan Li, Özlem Ceylan, Max Seifert, Filippo Nisic, Tuan Le Anh, Felix Meggendorfer, Claudia Dragonetti, Carlos-Andres Palma, Johannes V. Barth, and Jonathan J. Finley. A 2d semiconductor self assembled monolayer photoswitchable diode. *Advanced Materials*, 27(8):1426–1431, 2015.

[44] Daniel G. Walter, Dean J. Campbell, and Chad A. Mirkin. Photon gated electron transfer in two component self assembled monolayers. *The Journal of Physical Chemistry B*, 103(3):402–405, 1999.

[45] Li-Na Fu, Bing Leng, Yong-Sheng Li, and Xi-Ke Gao. Photoresponsive organic field effect transistors involving photochromic molecules. *Chinese Chemical Letters*, 27(8):1319 – 1329, 2016.

[46] Corinna Raimondo, NÃºria Crivillers, Federica Reinders, Fabian Sander, Marcel

Mayor, and Paolo Samori. Optically switchable organic field effect transistors based on photoresponsive gold nanoparticles blended with poly(3-hexylthiophene). *Proceedings of the National Academy of Sciences*, 109(31):12375–12380, July 2012.

[47] Nandita Biswas and Siva Umapathy. Density functional calculations of structures, vibrational frequencies, and normal modes of trans- and cis-azobenzene. *The Journal of Physical Chemistry A*, 101(30):5555–5566, 1997.

[48] Jeffrey M. Mativetsky, Giuseppina Pace, Mark Elbing, Maria A. Rampi, Marcel Mayor, and Paolo Samori. Azobenzenes as light-controlled molecular electronic switches in nanoscale metal molecule metal junctions. *Journal of the American Chemical Society*, 130(29):9192–9193, 2008. PMID: 18576645.